Ozone Monitoring Instrument (OMI)
Data User's Guide

OMI-DUG-3.0
December 3, 2009
Produced by OMI Team

This page is blank to preserve correct left-right pagination.

Contents

Chapter 1: Before You Begin

1.1 Purpose of the Document

Researchers and scientists in atmospheric sciences use this document to understand Ozone Monitoring Instrument (OMI) data and the OMI data products available. Most readers have with some background in atmospheric physics or chemistry, but not necessarily a strong background in remote sensing.

This guide provides the following:

1) Descriptions of the origin, advantages and limitations of the OMI.
2) Descriptions of OMI data products and their use.

The sources of information compiled for this document are listed in "Chapter 6: References," beginning on Page 55.

1.2 Acronyms, Abbreviations, and Definitions

AAOD	Aerosol Absorption Optical Depth
AOD	Aerosol Extinction Optical Depth
AERONET	Aerosol Robotic Network
AQUA	The First Member Satellite in A-Train Series
ATSR	Along Track Scanning Radiometer
BRD	Band Residual Difference
BUV	Backscatter Ultraviolet
CCD	Charge-Coupled Device
CMA	Center of Mass Altitude
DAAC	Distributed Active Archive Center
DEM	Detector Module
DU	Dobson Unit
ELU	Electronics Unit
EOS	Earth Observing System
EP	Earth Probe (satellite)
FOV	Field of View
FWHM	Full Width at Half Maximum
GDPS	Ground Data Processing System
GES DISC	Goddard Earth Sciences Data and Information Services Center
GEOS	Goddard Earth Observing System

GEOS-CHEM	A global three-dimensional model of atmospheric composition driven by assimilated meteorological observations from GEOS
GOME	Global Ozone Monitoring Experiment
HDF	Hierarchical Data Format, current level HDF5
HDF-EOS	The prescribed format for standard data products derived from EOS missions
IAM	Interface Adaptor Module
IFOV	Instantaneous Field of View
L0	Level 0 data are reconstructed, unprocessed instrument and payload data at full resolution, after the removal of all communications artifacts (for example, synchronization frames, communications headers, duplicate data). In most cases, the EOS Data and Operations System (EDOS) provides these data to the DAACs as production datasets for processing by the Science Data Processing Segment (SDPS) or by a SIPS to produce higher level products. **For more specific information about L0 through L3 data, refer to "**Chapter 3: OMI Data Products**" beginning on Page 13.**
L1A	Level 1A datasets consist of Level 0 data that have been time-referenced and annotated with ancillary information, including radiometric and geometric calibration coefficients and georeferencing parameters (for example, platform ephemeris) computed and appended but not applied to the Level 0 data.
L1B	Level 1B datasets consist of Level 1A data that have been processed to sensor units.
L2	Level 2 datasets contain derived geophysical variables at the same resolution and location as the Level 1 source data.
L2G	Level 2G datasets contain one day's worth of the Level 2 data (typically 14 orbits) ordered by ground position rather than by time.
L3	Level 3 data consists of L2 datasets with the variables mapped on uniform space-time grid scales, usually with some completeness and consistency.
LER	Lambertian-Equivalent Reflectivity
LF	Linear Fit
LIDAR	Light Detection and Ranging
LUT	Look-Up Table
MLER	Mixed Lambertian-Equivalent Reflectivity

MODIS	MODerate resolution Imaging Spectrometer
NIMBUS	A series of satellites for meteorological research
OA	Optical Assembly
OPB	Optical Bench
OMI	Ozone Monitoring Instrument
PBL	Planetary Boundary Layer
QF	Quality Flag
RMS	Root-Mean-Square (power measurement)
SBUV	Solar Backscatter Ultraviolet (instrument)
SC	Slant Column
SCO	Slant Column Ozone
SF	Spectral Fit
SIPS	Science Investigator-led data Processing System
SNR	Signal-to-Noise Ratio
SSA	Single Scattering Albedo
SZA	Solar Zenith Angle
TOMS	Total Ozone Mapping Spectrometer
UV	Ultra Violet
UVAI	UV Aerosol Index
VIS	Visible

Symbols:	**Definitions:**
σ	Standard Deviation
τ	Cloud Optical Depth

1.3 Overview of the Document

The chapters in this guide are described below:

Chapter 1 is the introduction to the guide.

Chapter 2 gives general information about the OMI.

Chapter 3 describes OMI data products in general.

Chapter 4 describes quality assessments of OMI Level 2 data products.

Chapter 5 describes OMI data format, data access and data usage.

Chapter 6 provides a reference list of source documents.

This page is blank to preserve correct left-right pagination.

Chapter 2: The Ozone Monitoring Instrument

2.1 Introduction to the OMI

OMI is a nadir-viewing near-UV/Visible CCD spectrometer aboard NASA's Earth Observing System's (EOS) Aura satellite. Aura flies in formation about 15 minutes behind Aqua, both of which orbit the earth in a polar Sun-synchronous pattern. Aura was launched on July 15, 2004, and OMI has collected data since August 9, 2004.

OMI measurements cover a spectral region of 264–504 nm (nanometers) with a spectral resolution between 0.42 nm and 0.63 nm and a nominal ground footprint of 13 × 24 km^2 at nadir. Essentially complete global coverage is achieved in one day. The significantly improved spatial resolution of OMI measurements as well as the vastly increased number of wavelengths observed, as compared to TOMS, GOME and SCIAMACHY, sets a new standard for trace gas and air quality monitoring from space. The OMI observations provide the following capabilities and features:

- A mapping of ozone columns at 13 km × 24 km and profiles at 13 km × 48 km (a continuation of TOMS and GOME ozone column data records and the ozone profile records of SBUV and GOME)
- A measurement of key air quality components: NO_2, SO_2, BrO, HCHO, and aerosol (a continuation of GOME measurements)
- The ability to distinguish between aerosol types, such as smoke, dust and sulfates
- The ability to measure aerosol absorption capacity in terms of aerosol absorption optical depth or single scattering albedo
- A measurement of cloud pressure and coverage
- A mapping of the global distribution and trends in UV-B radiation
- A combination of processing algorithms including TOMS Version 8, DOAS (Differential Optical Absorption Spectroscopy), Hyperspectral BUV retrievals and forward modeling to extract the various OMI data products
- Near real-time measurements of ozone and other trace gases

The OMI is a contribution of NIVR (Netherlands Institute for Air and Space Development) of Delft, in collaboration with FMI (Finnish Meteorological Institute), Helsinki, Finland, to the EOS Aura mission. The Dutch industrial efforts focused on the optical bench design and assembly, thermal design and project management. The detector modules and the readout and control electronics were provided by Finnish industrial partners.

2.2 The Aura Mission

Aura is the atmospheric chemistry mission of NASA's three-platform Earth Observing System (EOS) with the overall objective of studying the chemistry and dynamics of Earth's atmosphere from the ground through the mesosphere. The goal is to monitor the complex interactions of atmospheric constituents that are contributing to global change and to the creation and depletion of ozone. These atmospheric constituents are both from natural sources, such as biological activity and volcanoes, and from man-made sources, such as biomass burning,

The Aura satellite orbits at an altitude of 705 km in a sun-synchronous polar orbit with an exact 16-day repeat cycle and with a local equator crossing time of 13.45 (1:45 P.M.) on the ascending node. The orbital inclination is 98.1 degrees, providing latitudinal coverage from 82° N to 82° S.

Apart from OMI, the Aura satellite also carries onboard three other instruments: the High Resolution Dynamics Limb Sounder (HIRDLS), the Microwave Limb Sounder (MLS) and the Tropospheric Emission Spectrometer (TES). For more information about Aura and its instruments, refer to the Aura website (http://aura.gsfc.nasa.gov/). OMI calibration and validation information can be found in Dobber et al. (2006) and Froidevaux and Douglass (2001).

Algorithmic theoretical basis documents (ATBD) for OMI and other Aura instruments are available at http://eospso.gsfc.nasa.gov/eos_homepage/for_scientists/atbd/

2.3 OMI Mission Objectives

OMI's scientific mission (objectives discussed in detail by Levelt, et al., 2006) is directly related to the Aura mission objectives. The OMI mission seeks answers to the following questions:

- Is the ozone layer recovering as expected?
- What are the sources of aerosols and trace gases that affect global air quality and how are they transported?
- What are the roles of tropospheric ozone and aerosols in climate change?
- What are the causes of surface UV-B change?

2.4 OMI Description

2.4.1 Main Elements

OMI is composed of the following elements (graphically presented in Figure 1 below):

- Optical Assembly (OA), consisting of the Optical Bench (OPB), two Detector Modules (DEMs), and thermal hardware
- Electronics Unit (ELU), performing CCD readout control and analogue-to-digital conversion
- Interface Adaptor Module (IAM), performing Command Buffering as well as the Data Formatting and Satellite Bus Interface functions

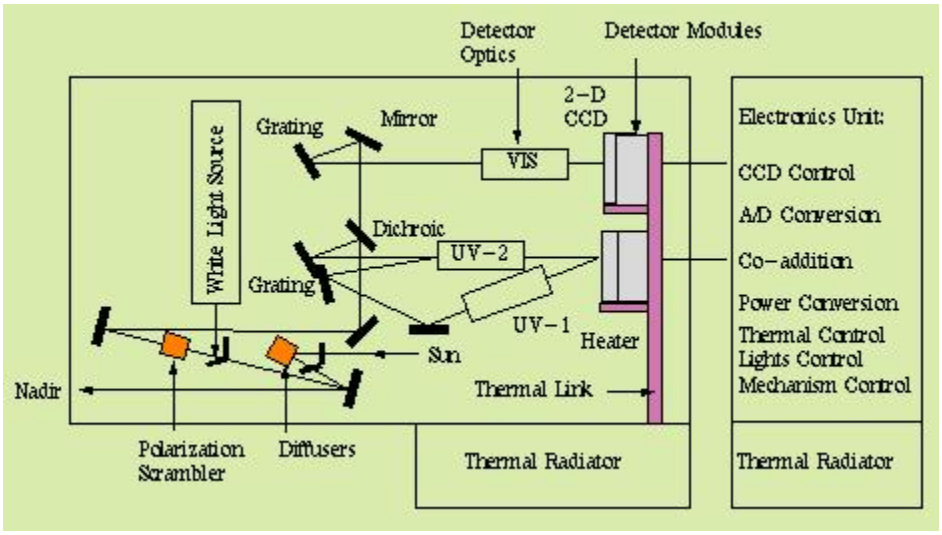

Figure 1: OMI Description

You can find a detailed OMI description at
http://www.knmi.nl/omi/documents/data/OMI_ATBD_Volume_1_V1d1.pdf
or at
http://www.knmi.nl/omi/documents/data/IEEE_OMI-Calibration_May2006.pdf

Table 1: General Description of OMI

Parameter	Value
Wavelength Range:	UV-1: 264-311 nm UV-2: 307-383 nm VIS: 349-504 nm
Spectral Resolution (FWHM):	UV-1: 0.63 nm UV-2: 0.42 nm VIS: 0.63 nm
Spectral Sampling (FWHM):	UV-1: 1.9 px UV-2: 3.0 px VIS: 3.0 px
Telescope FOV:	115º (2600 km on ground)
IFOV:	12 km × 6 km (flight direction × cross-flight direction)
Detector:	CCD: 780 × 576 (spectral × spatial) pixels
Mass:	65 kg
Duty Cycle:	60 minutes on daylight side 10-30 minutes on eclipse side (calibration)
Power:	66 watts
Data Rate:	0.8 Mbps (average)

2.4.2 Measurement Principle

OMI is a wide-angle, non-scanning and nadir-viewing instrument measuring the solar backscattered irradiance in a swath of 2600 km. The telescope Field of View (FOV) is 115º wide in across-track dimension. The instrument is designed as a compact UV/VIS imaging spectrograph, using a two-dimensional CCD array for simultaneous spatial and spectral registration (hyperspectral imaging in frame-transfer mode). The instrument has two channels measuring in the spectral range of 264-504 nm.

OMI employs a polarization scrambler that makes the instrument insensitive to the polarization state of the incoming radiance. The radiation is then focused by the secondary telescope mirror. A dichroic element separates the radiation into a UV and a VIS channel. The UV channel is split again into two subchannels: UV-1 (264-311 nm) and UV-2 (307-383 nm). In the UV-1 subchannel, the spatial sampling distance per pixel is a factor two larger than in the UV-2 subchannel. The idea is to increase the ratio between the useful signal and the dark current signal, and therefore increase the Signal-to-Noise Ratio (SNR) in UV-1, and to suppress the stray light below 300 nm. The resulting Instantaneous Field of View (IFOV) values of a pixel in the cross-track

direction are 12 km for UV-1 and 6 km for UV-2 and VIS. Groups of 4 or 8 CCD detector pixels are binned in the cross-track direction.

Five subsequent CCD images, each with a nominal exposure time of 0.4 s., are electronically co-added during a basic 2-second interval (the so-called "master clock period"). This results in an FOV of 13 km in the along-track direction. In addition, one column (wavelength) of each CCD data is downlinked without co-adding (monitoring of clouds, ground albedo). The pixel binning and image co-adding techniques are used to increase SNR and to reduce the data rate.

Images in the UV-1 channel have a 30-pixel resolution in the full cross-track direction, while those in the UV-2 and VIS channels have 60 pixels for the same full width. Details of these channels are provided in Table 2. For all the channels, the one-dimensional cross-track image is roughly perpendicular to the ground track and covers a distance of 2600 km on the earth's surface.

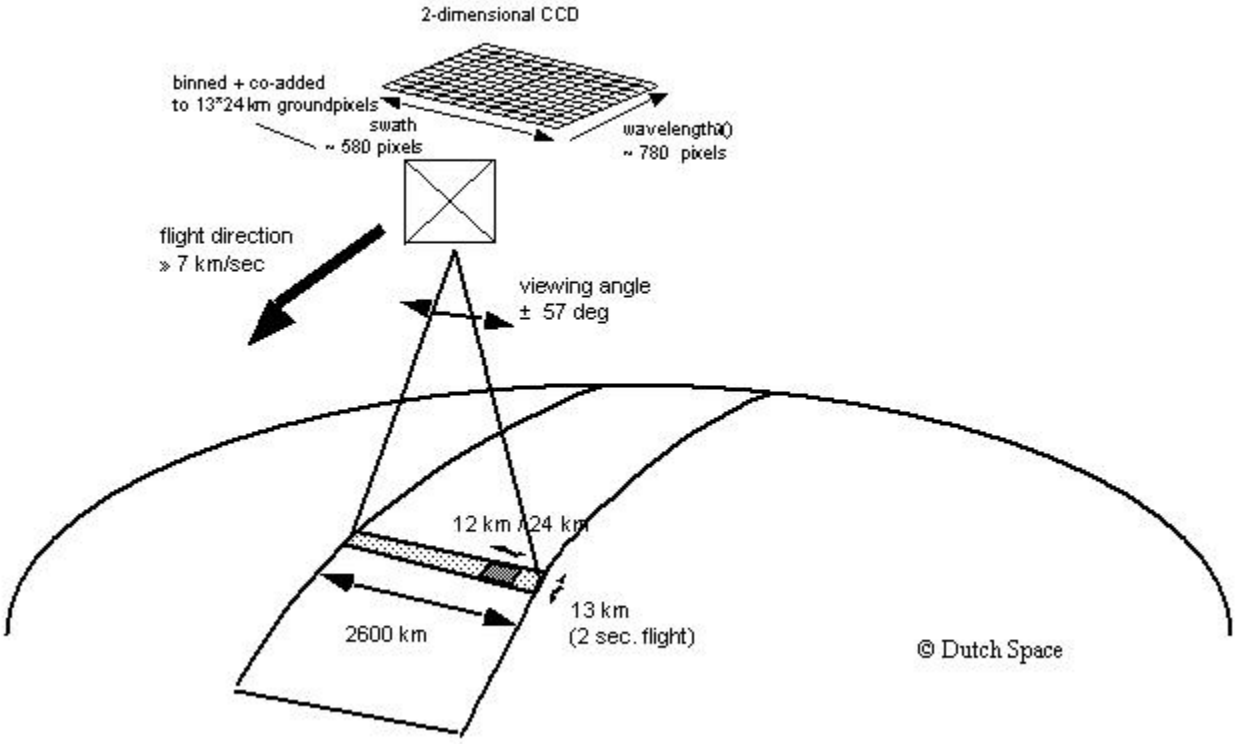

Figure 2: OMI Measurement Design

2.4.3 Observation Modes

OMI works in three different modes:

- Global mode
- Spatial zoom-in mode
- Spectral zoom-in mode

The global measurement mode is the default mode, sampling the complete swath of 2600 km for the complete wavelength range. The ground pixel size at nadir position in the global mode is 13 × 24 km^2 (along-track × cross-track) for the UV-2 and VIS channels, and 13 × 48 km^2 for the UV-1 channel.

The spatial zoom-in mode has a nadir ground pixel size of 13 × 12 km^2, but the swath width has a minimum of 725 km. The spatial zoom-in mode is used one day each 32 days, always above the same geo-locations. In the spectral range of 264-311 nm, the pixel size in the cross-track direction is twice as large (that is, a nadir ground pixel size of 13 × 24 km^2). The swath is symmetric with respect to the sub-satellite track. The spatial zoom-in mode results in two products:

- A Zoom Radiance product consisting of all the zoom data
- A Global Radiance product in which the zoom data are effectively degraded to match the resolution of images produced in the global mode but only cover half the normal mode radiance.

The spectral zoom-in mode has a nadir ground pixel size of 13 × 12 km^2 and a full swath of 2600 km. It has a limited spectral coverage of 307-432 nm to cover the most important scientific products. This mode was tested during the pre-launch period and run a few times between early August and early October 2004, during Launch and Early Operations (LEO). Because this mode has not been used since that time, it is not addressed in this document.

In Figure 3 below, the narrower swaths on the left-hand side of the image demonstrate retrievals from spatial zoom-in mode radiance measurements.

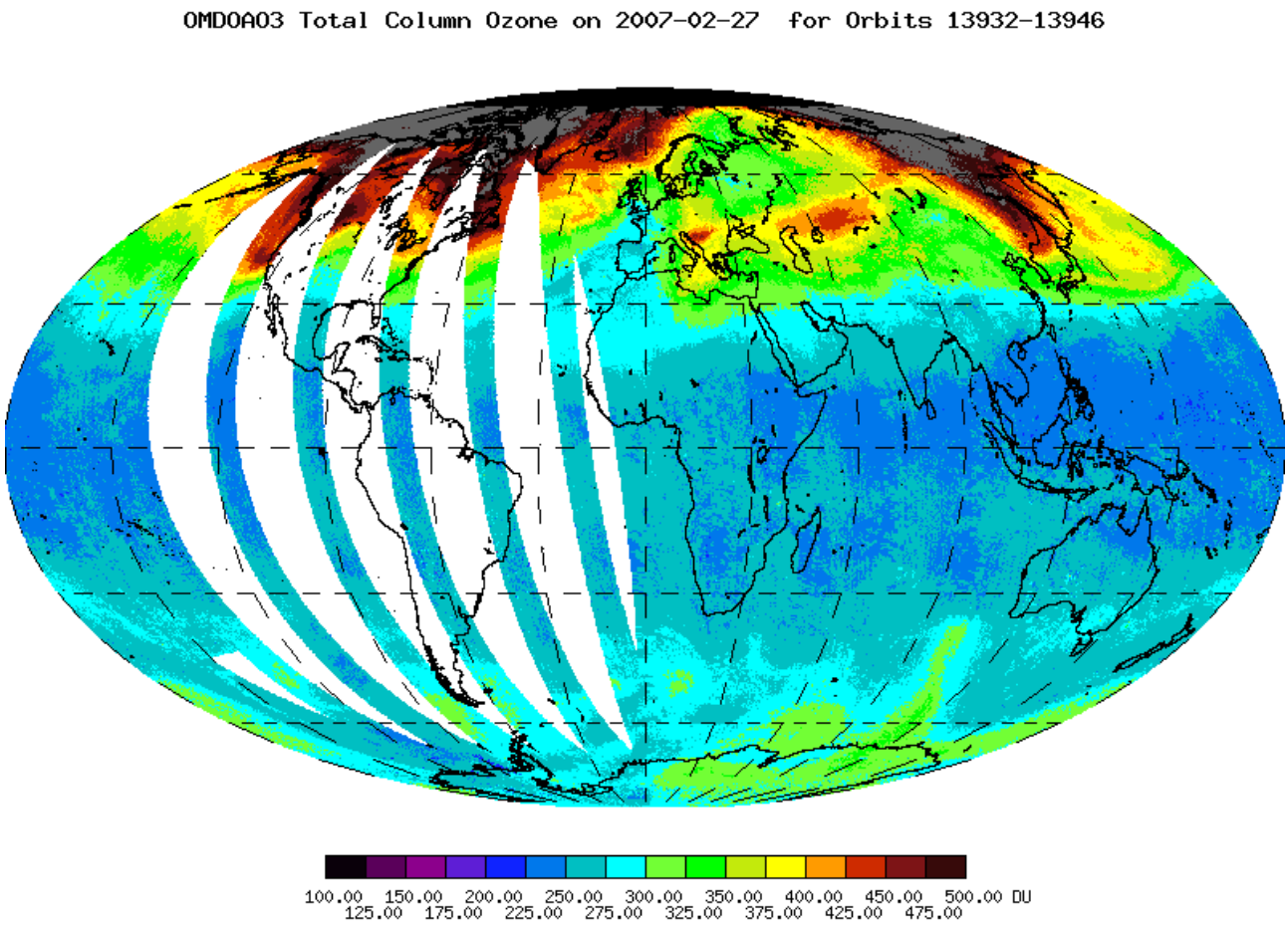

Figure 3: An Image of DOAS O_3 Product (OMDOAO3).

Table 2: Spectral Range, Resolution and Sampling Distances

Channel	Full Performance Range	Average Spectral Resolution (FWHM)	Average Spectral Sampling Distance
UV-1	264 – 311 nm	0.63 nm	0.33 nm/pixel
UV-2	307 – 383 nm	0.42 nm	0.14 nm/pixel
VIS	349 – 504 nm	0.63 nm	0.21 nm/pixel

Table 3: Characteristics of the Main Observation Modes

Observation Mode	Spectral Range	Swath Width Range	Ground Pixel Size at Nadir	Application
Global Mode				
UV-1	264 – 311 nm	2600 km	13 × 48 km^2	Global observation of all products
UV-2 & VIS	307-504 nm	2600 km	13 × 24 km^2	
Spatial Zoom-in Mode				
UV-1	264 – 311 nm	2600 km	13 × 24 km^2	Regional studies of all products
UV-2 & VIS	307-504 nm	725 km	13 × 12 km^2	

Chapter 3: OMI Data Products

3.1 OMI Data Processing and Product Summary

OMI data are processed at the OMI Science Investigator-led Processing System (SIPS) Facility in Greenbelt, Maryland, and are archived at the NASA Goddard Earth Sciences Data and Information Services Center (GES DISC). The OMI data products are available at four processing levels: Level 0, Level 1B, Level 2, and Level 3. For general information on OMI data products, refer to the document by Ahmad et al. (2003).

Level 0 products are raw sensor counts. Level 0 data are packaged into two-hour "chunks" of observations in the life of the spacecraft (and the OMI aboard it) irrespective of orbital boundaries. Level 1B processing takes Level 0 data and calibrates, geo-locates and packages the data into orbits.

Level 0, Level 1B, and Level 2 products contain orbital swath data, whereas Level 3 products contain global data that are composited over time (daily or monthly) or over space for small equal angle (latitude $\times$ longitude) grids covering the whole globe. The OMI data are implemented in the following 4 levels:

- Level 1B
- Level 2
- Level 2G
- Level 3

OMI Level 2 data files also contain temporal, spatial, solar, and viewing geometry parameters, quality flags, and extensive quality assurance information, in addition to the standard retrieved geophysical parameters. Sections 3.2 through 3.4 describe Standard Products. Section 3.5 describes existing Level 3 Special Products.

3.2 Level 1B Products: OMI Radiometrically Calibrated and Geo-located Radiance Products

The extensive calibration and data processing algorithm Ground Data Processing System (GDPS), was developed by Dutch Space in cooperation with the Dutch OMI team (Dobber et al, 2006; van den Oord et al., 2002; van den Oord et al., 2006). The Level 0 to 1B algorithm is used at OSIPS (NASA GSFC) to produce Level 1B OMI products. This algorithm takes the raw sensor measurements (Level 0 data), calibration, and spacecraft attitude and ephemeris information to produce radiometrically calibrated and geo-located radiances. There are six types of Level 1B Standard Products as shown in Table 4.

The lead scientist for Level 1B products is M. Dobber (dobber@knmi.nl). The calibration

website http://www.knmi.nl/omi/research/calibration publishes extensive daily reports and anomaly reports.

For more information about available Level 1B products, refer to the GES DISC's OMI Data page at:
http://disc.sci.gsfc.nasa.gov/Aura/OMI/index.shtml#L1B

Table 4. OMI Calibrated and Geo-located Earth View Radiance, Solar Irradiance, and Calibration Products (Level 1B)

	OMI Level 1B Calibrated Radiance & Irradiance (Orbital)
Product	**Product Description**
OML1BRUG	*Geo-located Earth View UV Radiance, Global-Mode Product* Geo-located earth view radiances from the UV channel detector in the wavelength range of 264-383 nm, using the global measurement mode. It also contains the data re-binned from the observations taken using zoom-in measurement modes.
OML1BRVG	*Geo-located Earth View VIS Radiance, Global-Mode Product* Geo-located earth view radiances from the VIS channel detector in the wavelength range of 349-504 nm, using the global measurement mode. It also contains the data re-binned from the observations taken using zoom-in measurement modes.
OML1BRUZ	*Geo-located Earth View UV Radiance, Zoom-in Mode Product* Geo-located earth view radiances from the UV channel detector in the wavelength range of 264-383 nm, using spectral and spatial zoom-in measurement modes.
OML1BRVZ	*Geo-located Earth View VIS Radiance, Zoom-in Mode Product* Geo-located earth view radiances from the VIS channel detector in the wavelength range of 349-504 nm, using spectral and spatial zoom-in measurement modes.
OML1BIRR	*Solar Irradiance Product* Averaged sun measurements of the solar irradiances from both the UV and VIS channel detectors over a single solar observation in the wavelength range of 264-504 nm. Contains solar measurement data products for both the global and the spatial zoom-in mode. This product only contains measurement data obtained with the quartz volume diffuser.
OML1BCAL	*Calibration Data* In-flight calibration measurement results, including the complete CCD readouts for both the UV and VIS channels from the areas on the CCD that are intended for calibration purposes (which is outside of the area normally used by the spectrometer). All White Light Source (WLS) and LED measurements are also stored in this product. Solar measurement data from all three on-board diffusers is stored in the calibration data product.

3.3 Level 2 Products: OMI Orbital Atmospheric Products

The OMI Level 2 (orbital swaths) products contain the geophysical parameters (at ground-pixel resolution) derived from radiometrically calibrated and geo-located radiances (Level 1B product). Refer to Table 5 below for the spectral radiances used for the retrieval of OMI products.

Each Level 2 product file consists of parameters retrieved from observations made only in the daytime portion of an orbit (~ 53-minute duration). In addition to standard derived parameters, these files also contain some auxiliary derived parameters, ancillary input parameters, temporal, spatial, solar and viewing geometry, terrain height, ground-pixel quality flags, and extensive quality assurance information. In the OMI global operational mode, the spatial resolution is 13 × 24 km^2 at nadir.

Almost all Level 2 products contain data at 13 × 24 km^2 (nadir pixel size) resolution with the exception of zoom-in products and the ozone profile product. Level 2 products are available at higher spatial resolution using the OMI spatial zoom-in mode data at 13 × 12 km^2 resolution. These products' short names end with a *Z* (for zoom-in). The ozone profile product will be available with a spatial resolution of 13 × 48 km^2.

Table 5. OMI Level 2 Product Description

Product Description	Acronym	Spectral Range (nm)	Release Dates	Granule File Size in (MB)
Surface spectral irradiance & Erythemally weighted UV Flux	OMUVB	305, 310, 324, 380	April 20, 2007	10
Ozone column: DOAS method	OMDOAO3	331.1-336.1	June 26, 2006	11
Ozone column: TOMS Version 8 method	OMTO3	317.5, 331.2, 360	April 29, 2005	48
Aerosol: near-UV algorithm	OMAERUV	354-388	August 31, 2006	6
Aerosol: multi-wavelength algorithm	OMAERO	331-500	November 23, 2007	10
Cloud Fraction and Cloud Pressure: O_2-O_2 absorption method	OMCLDO2	477	June 26, 2006	15
Cloud Fraction and Cloud Pressure: Rotational Raman method	OMCLDRR	346-354	April 20, 2006	6

Product Description	Acronym	Spectral Range (nm)	Release Dates	Granule File Size in (MB)
O_3 Profile	OMO3PR	270-330	September 9, 2009	11
SO_2	OMSO2	310.8-314.4 345-370	December 20, 2006	21
HCHO	OMHCHO	325-357	February 1, 2007	5
BrO	OMBRO	338-357	February 1, 2007	5
OClO	OMOCLO	366-401	February 1, 2007	5
NO_2	OMNO2	405-465	September 29, 2006	17

Level 2 products consist of the products in the different categories:

- Ozone products
- Clouds, Aerosols and Surface UV Irradiance products
- Trace Gases products

3.3.1 Ozone Products

There are three Level 2 (L2) ozone products based on the algorithms that originated from the Total Ozone Mapping Spectrometer (TOMS), the Global Ozone Monitoring Experiment (GOME), and the Scanning Imaging Absorption Spectrometer for Atmospheric CHartographY (SCIAMACHY). These ozone products provide column ozone and ozone profiles.

Two algorithms are available for the total ozone retrieval: the enhanced TOMS Version 8 (V8) algorithm used to process all 25 years of TOMS data and the Differential Optical Absorption Spectroscopy (DOAS) technique used with GOME and SCIAMACHY ozone retrievals. The TOMS V8 algorithm retrieves vertical column ozone data essentially using 317.5 and 331.2 nm wavelengths (Bhartia et al., 2008; Balis, D., M. Kroon, M. E. Koukouli, E. J. Brinksma, G. Labow, J. P. Veefkind, and R. D. McPeters (2007), Validation of Ozone Monitoring Instrument total ozone column measurements using Brewer and Dobson spectrophotometer ground-based observations, *J. Geophys. Res.*, 112, D24S46, doi:10.1029/2007JD008796.

Bhartia and Wellemeyer, 2002). OMI's additional hyperspectral measurements provide better estimates and corrections of the factors that induce uncertainty in ozone retrieval (for example, cloud and aerosol, sea-glint effects, profile shape sensitivity, SO_2 and other trace gas contamination). The DOAS technique is based on the fitting of the satellite-measured gases absorption structure at the number of absorption lines in the spectral

region 331.1-336 nm to the gases absorption structure measured in the laboratory (Veefkind et al., 2002; Veefkind et al., 2006). Slant column density is determined first and then is translated into vertical column density using an air mass factor, which is computed using radiative transfer models.

Table 6. OMI Ozone Products (Level 2)

OMI Ozone (Total column & Profile)		
Product	**Parameters**	**Lead Scientist**
OMTO3	O_3 total column (TOMS V8 method), also other derived and ancillary parameters including N-values, effective Lambertian scene-reflectivity, UV aerosol index, SO_2 index, cloud fraction, terrain and cloud pressure, ozone below clouds, geo-location, solar and satellite viewing angles, and quality flags.	P.K. Bhartia Pawan.K.Bhartia@nasa.gov
OMDOAO3	O_3 total column (DOAS method), ozone slant column density and its precision (for data assimilation), also other derived and ancillary parameters including ozone ghost column density, air mass factor (all, clear, and cloudy scenes), scene reflectivity, radiance over the DOAS fit window (331.1 to 336.1 nm), root mean square of DOAS fit, cloud fraction, cloud radiance, terrain and cloud pressure, geo-location, viewing angles, and quality flags.	J.P. Veefkind veefkind@knmi.nl
OMO3PR	O_3 profile (optimum estimation method), ozone profile error covariance matrix, ozone a-priori profile, ozone a-priori error covariance matrix, ozone averaging kernel, number of iterations, pressure levels for the layers, temperatures at the interfaces between the layers, altitude grid for the layers, latitude, longitude, viewing direction and solar position. This product comes from the Royal Meteorological Institute (Dutch: *Koninklijk Nederlands Meteorologisch Instituut*, KNMI).	J.F. de Haan johan.de.haan@knmi.nl

Ozone profile retrieval is based on the Optimal Estimation method (also referred to as Rodger's maximum-likelihood estimation technique), uses all ozone sensitive wave-lengths' radiances (in spectral region 270 to 330 nm), a priori ozone profile, radiances, and a Jacobian matrix computed from the LABOS radiative transfer model. Hyperspectral capabilities provide better vertical resolution below 20 km compared to the Solar Backscatter Ultraviolet instrument (SBUV), which has 12 wavelengths, not all of which are used to determine profile ozone.

3.3.2 Clouds, Aerosols and Surface UV Irradiance Products

OMI produces cloud fraction and cloud pressure measurements that are used in OMI trace-gas retrievals and in the retrieval of data products from other Aura sensors. The two methods used for the cloud pressure retrieval are the O_2-O_2 absorption method and the Rotational Raman Scattering (RRS) method. The O_2-O_2 absorption method is based on spectral fitting of O_2-O_2 absorption band at 477 nm using the Differential Optical Absorption Spectroscopy (DOAS) technique (Acarreta and de Haan, 2002; KNMI website: http://www.knmi.nl/omi/research/documents/). The RRS method is based on the least square fitting of the ring spectrum (Joiner, et al., 2002; 2006; Vasilkov et al., 2004).

Users should be aware that both the cloud pressure and fraction derived from both OMI algorithms are effective, meaning that the cloud fraction may not represent true geometrical cloud fraction and that cloud pressure may not represent a true cloud top pressure.

The cloud fraction is determined such that the average top of atmosphere reflectance over the fit window is reproduced with a Lambertian reflector. The pressure of this Lambertian cloud is adjusted to reproduce the intensity of the pressure sensitive feature (the depth of the O_2-O_2 absorption near 475 nm or the amount of filling in of the Fraunhofer lines in the solar spectrum by rotational Raman scattering). Model studies and limited comparisons with CloudSat have shown that this pressure level is generally well within the cloud.

OMI also provides aerosol information needed by other Aura algorithms. Two algorithms (near-UV and multi-wavelength methods) are used for the retrieval of aerosol characteristics over the ocean and land (Torres et al., 2002; Veihelmann et al., 2007). The availability of the near-UV wavelengths also makes the aerosol retrieval over the desert area possible since the land reflectance is small at these wavelengths. In addition to providing information on the aerosol absorption and single scattering albedo, OMI aerosol algorithms can differentiate between sulfate, smoke and dust aerosols, and characterize the type of urban aerosols. The aerosol index (a side product of the near-UV method) is used for detection of absorbing aerosols even in cloudy scenes and above snow/ice surfaces.

The spectral surface irradiance (at 305, 310, 324, and 380 nm) reaching the ground and erythemally weighted irradiance (covering 290-400 nm) are produced using the enhanced version of TOMS Surface UV-B flux algorithm (Krotkov et al., 1998; 2001; 2002; Tanskanen et al., 2007).

Measured earth-atmosphere radiances are used in conjunction with the radiative transfer model to retrieve UV spectral irradiances reaching the ground. The OMI algorithm uses actual snow thickness information from the European Centre for Medium-Range Weather Forecasts (ECMWF) analysis, which improves the accuracy of the values for the high latitudes.

The erythemal UV exposure is calculated using a model for the susceptibility of Caucasian skin to sunburn (erythemal). Table 7 also provides some highlights of clouds, aerosols and surface irradiance exposure products.

Table 7. OMI Clouds, Aerosols, and Surface UV Exposure Products (Level 2)

Clouds		
Product	**Parameters**	**Lead Scientist**
OMCLDO2	Cloud fraction and cloud pressure (O_2-O_2 absorption method), slant column O_2-O_2 and O_3, ring coefficients, and uncertainties in derived parameters, terrain and geo-location information, solar and satellite viewing angles, and quality flags.	J.F. de Haan johan.de.haan@knmi.nl
OMCLDRR	Cloud fraction and cloud pressure (Rotational Raman scattering method), other derived and ancillary parameters, terrain and geo-location information, solar and satellite viewing angles, and quality flags.	J. Joiner Joanna.Joiner-1@nasa.gov
Aerosols over Ocean and Land		
OMAERO	Aerosol characteristics such as aerosol optical thickness, aerosol indices, aerosol type, as well as ancillary information. The aerosol type gives an indication about the single scattering albedo, the layer height, and the size distribution.	Pepjin Veefkind veefkind@knmi.nl
OMAERUV	UV aerosol index (UVAI), aerosol extinction optical depth (AOD), and aerosol absorption optical depth (AAOD) and single scattering albedo (SSA).	O. Torres omar.torres@hamptonu.edu
Surface UV-Irradiance		
OMUVB	Surface erythemal UV exposure (TOMS algorithm): downward spectral irradiances ($W/m^2/nm$) at the ground for 305, 310, 324, and 380 nm; erythemally weighted UV irradiance (W/m^2) covering 290-400 nm spectral region (noontime values and daily averages). This product is produced at FMI (Finland), and is archived at NASA GES DISC as a standard product.	Antti Arola antti.arola@fmi.fi

3.3.3 Trace Gases Products

Total column and slant column values of trace gases, NO2, BrO, HCHO, OClO, and SO2 are produced by fitting absorption spectra. (Chance et al., 2002; Boersma et al., 2002; Krotkov et al., 2006; Krotkov et al., 2008; Yang et al., 2007 ; Krueger et al., 2002). Table 8 provides highlights of these products. The OMI algorithm detects volcanic ash and sulfur dioxide produced in volcanic eruptions with up to 40 times more sensitivity than TOMS and GOME (Krueger et al., 2002).

Table 8. OMI Trace Gases Products (Level 2)

Trace Gases (NO_2, BrO, HCHO, OClO, and SO_2)		
Product	**Parameters**	**Lead Scientist**
OMNO2	NO_2 total and tropospheric column, slant column density, one sigma fitting uncertainties for the NO_2 and the other species varied in the fitting window, correlation of other fitted species to the NO_2, fitting root mean square (rms), surface reflectivity, cloud top height, geo-location, and solar and satellite viewing angles.	J. Gleason James.F.Gleason@nasa.gov J.P. Veefkind veefkind@knmi.nl
OMBRO	BrO total column and slant column abundance, one sigma fitting uncertainties for the BrO and the other species varied in the fitting window, correlation of other fitted species to the BrO, fitting RMS, surface reflectivity, cloud top height, quality flags, geo-location, and solar and satellite viewing angles.	K. Chance kchance@cfa.harvard.edu
OMHCHO	HCHO total column and slant column abundance, one sigma fitting uncertainties for the HCHO and the other species varied in the fitting window, correlation of other fitted species to the HCHO, fitting RMS, surface reflectivity, cloud top height, quality flags, geo-location, and solar and satellite viewing angles.	K. Chance kchance@cfa.harvard.edu
OMOCLO	OClO slant column and one sigma fitting uncertainties for the OClO and the other species varied in the fitting window, correlation of other fitted species to the OClO, fitting RMS, surface reflectivity, cloud top height, quality flags, geo-location, and solar and satellite viewing angles. Note that this product is not global (retrieved for polar regions only).	K. Chance kchance@cfa.harvard.edu

Trace Gases (NO_2, BrO, HCHO, OClO, and SO_2)		
OMSO2	Total SO_2 (vertical column in Dobson Units, where 1DU=2.69 $\times$ 10^{16} molecules/cm^2), in the PBL, lower and middle troposphere, and in lower stratosphere corresponding to different sources: fossil fuel combustion, smelters, volcanic degassing, and volcanic eruptions. Adjustments to OMTO3 total ozone and Lambertian equivalent UV reflectivity spectral dependence and ancillary information (satellite geometry, quality flags, geo- location).	N. Krotkov Nickolay.A.Krotkov@nasa.gov

3.4 Level 2G Products: OMI Global Binned Atmospheric Products

Level 2G (L2G) datasets contain one day's worth of the Level 2 data (typically 14 orbits) ordered by ground position rather than by time. Only the most relevant L2 fields are included in the L2G. In an L2G dataset, each of the pixels from the included L2 files is assigned to a point on a 0.25 by 0.25 degree latitude/longitude grid (with exception for OMSO2G where 0.125 by 0.125 degree latitude/longitude grid is used). By precise definition, however, this is not a gridded product because pixels from different L2 datasets are not combined in any way; that is, all L2 pixels are included in the dataset. The transformation into a L2G dataset is reversible (able to be taken back to L2 data) because there is sufficient information stored in the L2G dataset to reproduce the L2 data used to generate it.

L2G datasets are often smaller than the sum of the parts, due in part to data fields that have been dropped, but also due to more efficient use of internal Hierarchical Data Format (HDF5) compression. Users do not need to take any extra steps to use datasets to which internal HDF5 compression has been applied.

The L2G datasets offer a number of benefits, specifically:

- They require equal or less storage space than the 14 or so L2 files used to generate them.
- They reduce by a factor of 14 the number of files in your directories when storing one or more days' worth of consecutive data.
- They reduce by a factor of 14 the number of files your analysis code needs to open when processing one or more days' worth of consecutive data.
- They facilitate gridded (Level 3) product generation.
- They facilitate geographic subsetting.

L2G products have been generated or released for all L2 standard products except OMBRO, OMOCLO.

3.5 Level 3 Products: OMI Global Gridded Atmospheric Products

Each Level 2 product file contains data from a single orbit. For each Level 2 product there are 14 files per day. OMI Level 3 daily global products are produced by using best pixel data over small equal angle grids (0.25 degree × 0.25 degree), (0.5 degree × 0.5 degree) or (1 degree × 1 degree) covering the whole globe. Each grid also contains the corresponding statistical parameters (number of pixels, minimum, maximum, and standard deviation).

At the time of this printing, Level 3 (Level 3d - 1 degree × 1 degree; Level 3e – 0.25 degree × 0.25 degree) products are available for many OMI standard products (OMAERUVd, OMAEROe, OMNO2e, OMSO2d, OMDOAO3e, OMTO3d, OMTO3e, OMUVBd).

Apart from above standard products, Level 3 surface reflectance product OMLER is available in 0.5 degree × 0.5 degree grid. For more on this product, refer to

http://disc.gsfc.nasa.gov/Aura/OMI/omler_v003.shtml.

Chapter 4: Quality Assessment of OMI Level 2 Products

Currently, all products are available as Version 3 products that are based on better calibrated radiances.

4.1 OMI Pixel Size

Understanding pixel shape and size is an important aspect of assessing the quality of data products. A single Level 2 product file contains all OMI measurements on the sunlit portion of the Earth, for a single Aura orbit. During one orbit, OMI performs approximately 1650 measurements, which take 2 seconds each. In the global observation mode, 60 cross-track ground pixels are measured simultaneously during each measurement. These 60 measurements cover a swath approximately 2600 km wide.

Figure 4 shows the pixel size and orientation across the scan for the two UV channels. Due to curvature of the Earth and the slight asymmetric alignment between the instrument's optical axis and the spacecraft axes, the ground pixels are not symmetrically aligned with respect to the orbital plane. (Note that the latitude and longitude cover different distances on the Earth's surface.) The satellite trajectory in this figure is in the direction of increasing latitude. The following pixel dimensions and sizes were computed at the Earth's surface on the WGS84 ellipsoid.

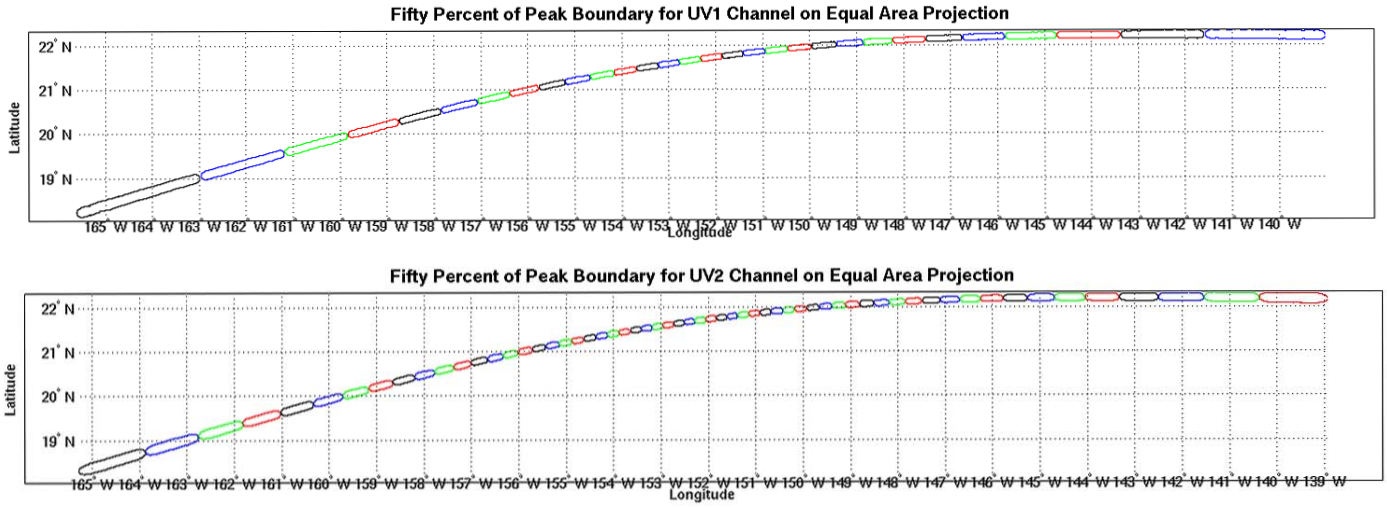

Figure 4: The Position of 60 Ground Pixels for an OMI Measurement

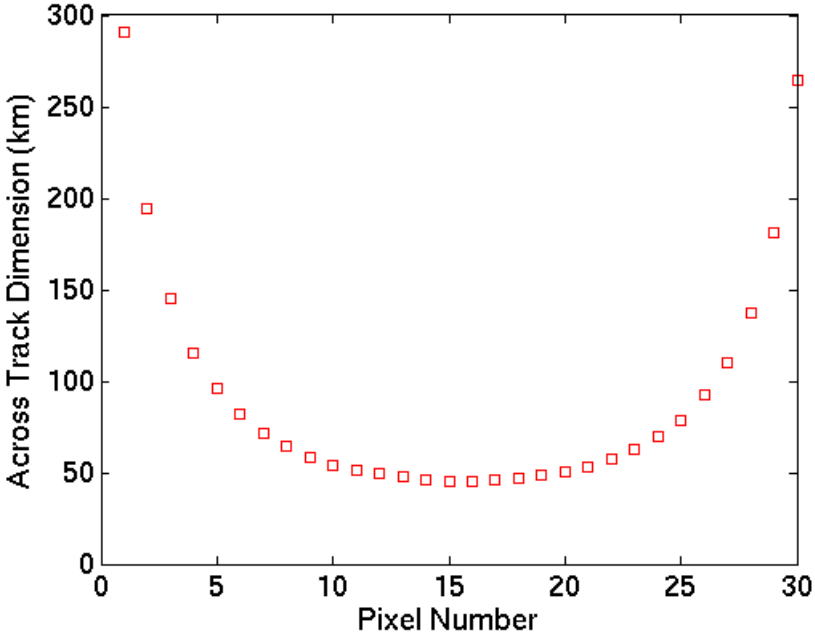

Figure 5: UV1 Cross-Track Dimension Versus Scan Position

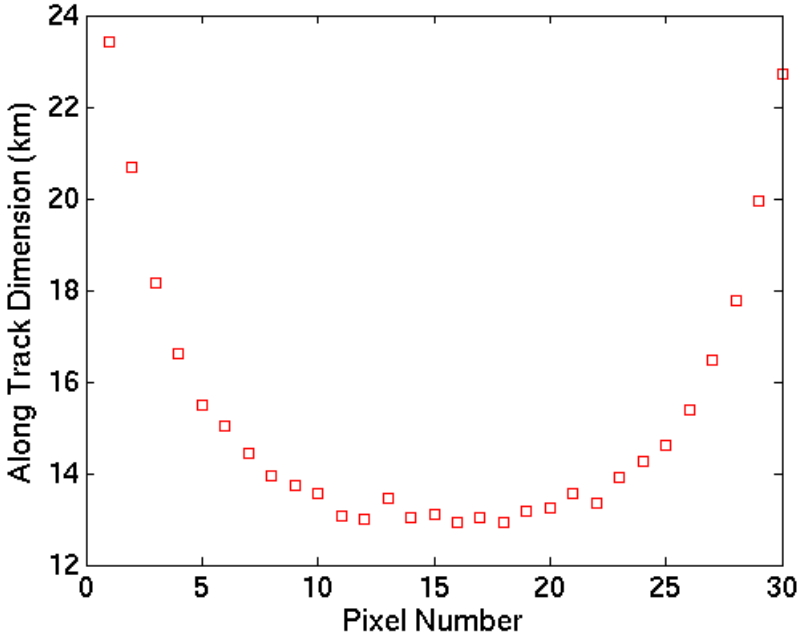

Figure 6: UV1 Along-Track Dimension Versus Scan Position

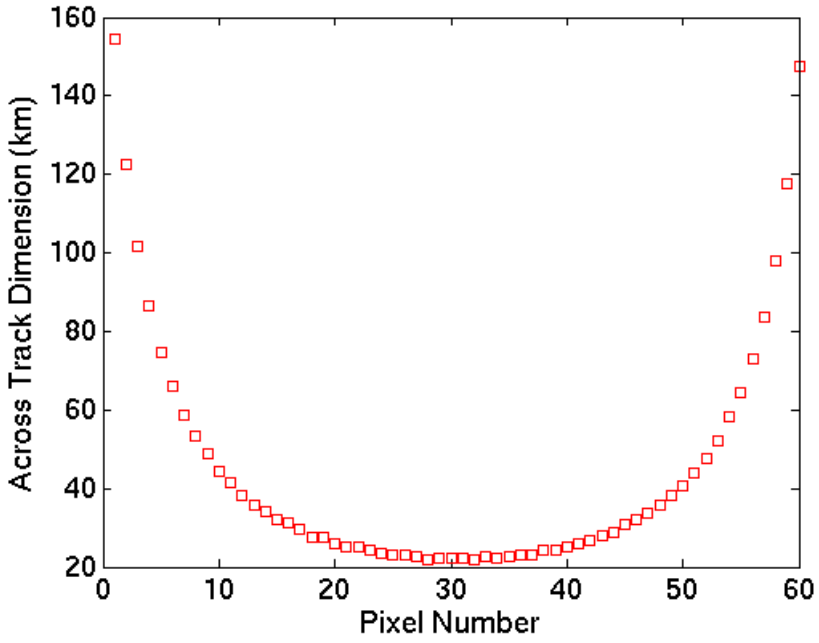

Figure 7: UV2 Cross-Track Dimension Versus Scan Position

Note: The above and below pixel representations show UV2, but the graphs of UV2 and VIS are virtually identical.

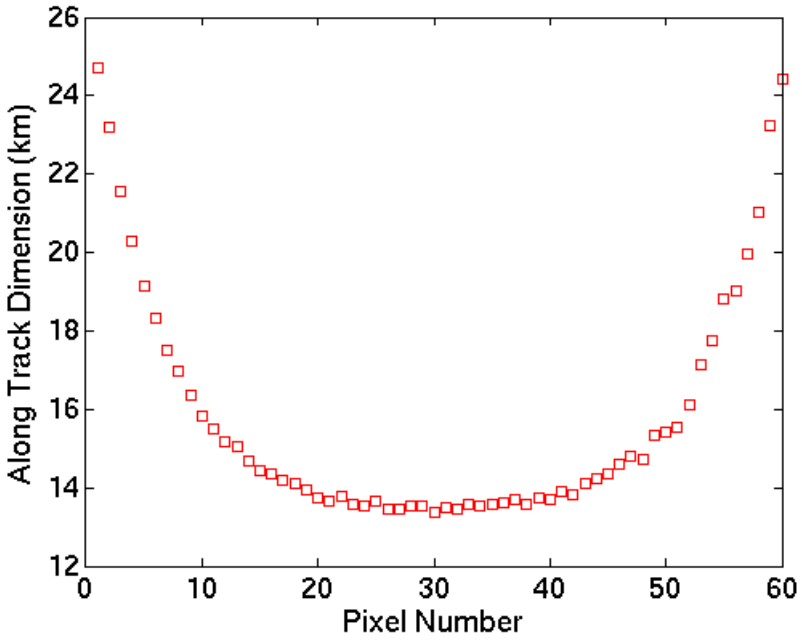

Figure 8: UV2 Along-Track Dimension Versus Scan Position

The following table shows the pixel size at the different scan locations:

Table 9: Pixel Size at Different Scan Locations

Scan Position	*UV1 Pixel Size (km^2)*	*UV2 Pixel Size (km^2)*	*VIS Pixel Size (km^2)*
1	7062.2	3799.4	3800.6
2	4152.2	2803.2	2806.7
3	2775	2168.3	2171.8
4	2040.9	1742	1738.5
5	1586.7	1432.1	1430.9
6	1302.8	1207.9	1209
7	1105.3	1034.1	1036.4
8	968.34	908.16	903.52
9	869.7	803.36	799.89
10	793.16	716.13	719.59
11	742.07	650.99	652.14
12	703.72	596.37	598.67
13	687.27	551.06	548.75
14	661.69	515.04	515.04
15	649.9	480.24	481.38
16	647.32	452.39	448.93
17	659.64	429.18	430.32
18	671.98	402.55	406
19	694.61	392.05	389.75
20	730.97	371.22	373.52
21	778.76	358.46	360.75
22	840.25	356.05	354.89
23	931.43	342.16	346.75
24	1061.4	335.17	335.17
25	1233.7	329.34	328.19
26	1496.1	323.51	326.95
27	1899	317.7	321.14
28	2556.4	317.62	316.47
29	3736.8	317.54	317.54
30	6170.2	310.59	307.15
31		316.25	313.96
32		313.89	312.74
33		321.84	320.69
34		318.34	316.05
35		324	321.71
36		331.95	331.94

Scan Position	*UV1 Pixel Size (km^2)*	*UV2 Pixel Size (km^2)*	*VIS Pixel Size (km^2)*
37		331.89	335.31
38		339.83	339.83
39		350.07	347.77
40		355.73	356.87
41		372.82	372.81
42		381.9	384.19
43		404.71	404.71
44		418.37	421.79
45		448.02	446.87
46		470.81	471.95
47		503.89	505.03
48		533.53	539.24
49		584.88	581.45
50		635.08	629.36
51		687.56	697.83
52		772.01	777.71
53		880.44	870.15
54		1011.7	1012.8
55		1183	1181.8
56		1378.2	1401
57		1654.5	1655.6
58		2047.3	2046.2
59		2652.7	2641.2
60		3554.1	3562

In Figure 9 below, the plot of the 50% power response curve is plotted in black.

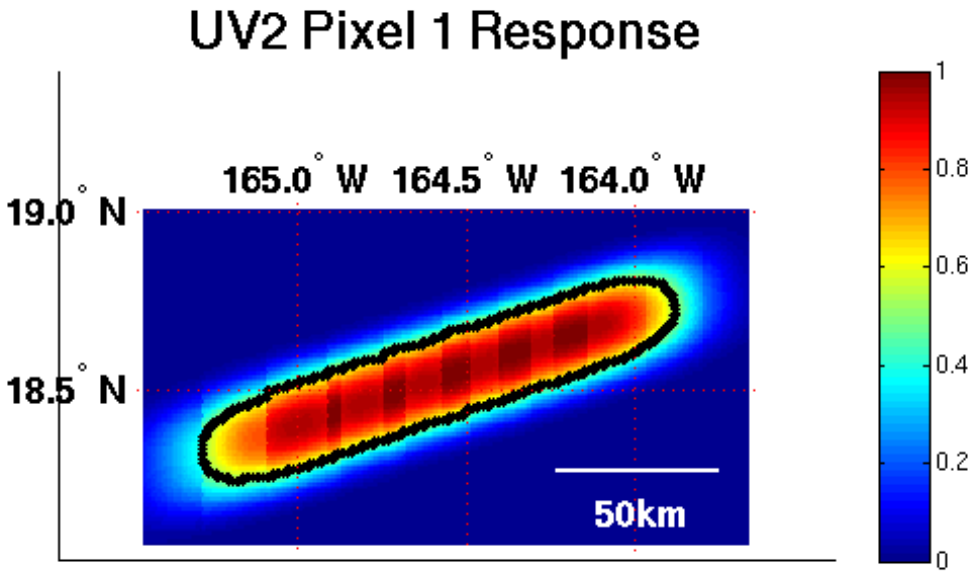

Figure 9: Approximation of Pixel Shape

During zoom-in measurements, the swath width may be reduced. The operational baseline includes zoom-in measurements for one day a month. With zoom-in measurements, 30 of the 60 cross-track pixels contain data; the other 30 contain fill values.

Each Level 2 file contains data from the day lit portion of an orbit (~53 minutes). There are approximately 14 orbits per day. A Level 2 product file is written as an HDF-EOS5 swath file.

Refer to Chapter 3, Table 5, for a summary of the products, and to Tables 6 through 8 for the product descriptions.

Questions related to Level 2 datasets should be directed to the GES DISC (help-disc@listserv.gsfc.nasa.gov). You are strongly advised to consult the OMI Quality Assurance Team (omiqa@ltpmail.gsfc.nasa.gov) for most recent information on the assessment of data quality.

4.2 OMI/Aura Aerosol Extinction Optical Depth and Aerosol Types (OMAERO)

4.2.1 Quality Assessment

Various validation studies have been made or are in progress for the aerosol optical thickness from the OMAERO product using ground based, airborne, and satellite based observations. Note that the results of current validation studies for land scenes are affected by issues related to the currently used surface albedo climatology. The validation

studies for land will be updated and extended once the new surface albedo climatology from OMI data is implemented.

For ocean scenes, global AOD data from the OMAERO product have been compared with measurements from other satellite instruments. Here we show such a comparison for the period of June 2006.

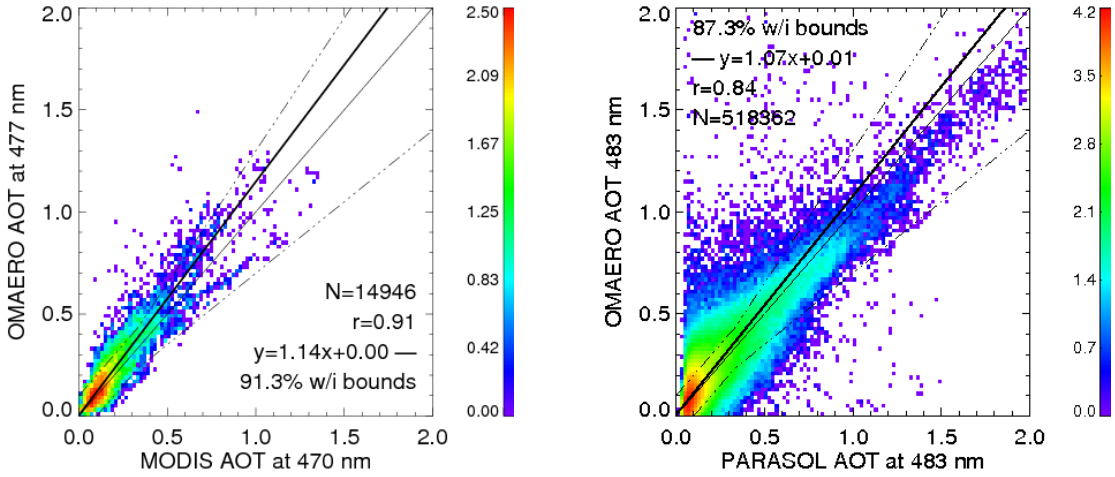

Figure 10: AOT from the OMAERO product compared with quality-assured data from the MODIS standard product (left) and with quality parameter-filtered data from POLDER (right)

The comparison with quality assured data from the MODIS standard product (Figure 10, left) shows excellent agreement between the datasets. For this comparison only quality assured MODIS data (QA flag=3) have been included. By using this data flag many partly clouded OMI scenes are excluded that are not recognized as being cloudy by the OMI cloud screening scheme. When OMI data are used alone, unrecognized cloud contamination is an important source of errors. For the comparison with POLDER on the PARASOL platform, the data have been filtered based on the quality parameter given by the POLDER aerosol algorithm. A correlation coefficient of larger than 0.8 and a slope of the regression line of 1.07 indicate a good agreement between the datasets.

For land scenes, we report the results of various validation studies. Curier, et al. (2007) have investigated the AOD data from the OMAERO product for Europe and adjacent oceans. A comparison with MODIS AOD data yields correlation coefficients between 0.76 and 0.81 for ocean and between 0.59 and 0.70 for land. The difference between land and sea is due to shortcomings in the currently used surface albedo climatology. In the same study strongly site-dependent correlations are reported for comparisons of the AOD from the OMAERO product with ground based data from various AERONET stations in Europe.

The level 2 product contains diagnostic information about the quality of the fit. Typical values for the retrieval error of the AOD obtained using the non-linear fitting routine are below 0.03. This error concerns the AOD retrieval for a given aerosol model and hence does not include error correlations of AOD and microphysical aerosol parameters or the aerosol height. The standard deviation of the AOD values of the aerosol models with a Root Mean Square (RMS) error lower than a given threshold is below 0.11 for 95% of the cases. The standard deviation of the Single Scattering Albedo (SSA) values of the aerosol models with an RMS lower than a given threshold is below 0.1 in 95% of the cases.

4.2.2 Additional Information

Direct questions related to the OMAERO dataset to help-disc@listserv.gsfc.nasa.gov. For questions and comments related to the OMAERO algorithm and data quality, please send an e-mail to omaero@ltpmail.gsfc.nasa.gov.

For more information on this product, refer to:
http://disc.gsfc.nasa.gov/Aura/OMI/omaero_v003.shtml

4.3 OMI/Aura Near-UV Aerosol Absorption and Extinction Optical Depth and Single Scattering Albedo (OMAERUV)

4.3.1 Quality Assessment

A very important parameter that is reported in the quality assessment of OMAERUV data is the algorithm quality flag (field name AlgorithmFlags), which contains the processing error flag in its first byte. A detailed description of the data quality flags is given in the OMAERUV readme file http://disc.sci.gsfc.nasa.gov/Aura/data-holdings/OMI/documents/v003/OMAERUV_README_V003.doc. Most users should use data with a data quality flag 0 or 1.

Because of the relatively large footprint of the OMI observations (13x24 km^2 at nadir), the major factor affecting the quality of aerosol products is sub-pixel cloud contamination. Currently the cloud mask is based on simple reflectivity and UVAI thresholds, which can cause significant overestimation of the mean AOD. However, experience with TOMS suggests that monthly mean AODs do reliably capture variation in the AOD with time. It is important to note, however, that the AAOD is less affected by cloud contamination and hence is more reliable.

In general OMAERUV retrievals are more reliable over land than over water surfaces. The near-UV retrieval method is particularly sensitive to carbonaceous and mineral aerosols. The sources of these aerosol types are located over the continents, and the atmospheric aerosol load associated with these events is generally large. In addition, dust and smoke aerosol events tend to take place under meteorological conditions which do not favor the formation of clouds in the vicinity of the sources, such as arid and semi-arid

areas in the case of dust, and the dry season in the case of biomass burning. The OMAERUV retrieved AOD of sulfate-based aerosols is less accurate due to its low values, higher spatial variability and increased levels of sub-pixel cloud contamination.

Ocean OMAERUV retrievals are affected by other factors. In addition to sub-pixel clouds, the ocean surface reflectance has both angular and spectral variations, the latter due to spectrally varying scattering from the water, often called water-leaving radiances (WLR). Chlorophyll, sediments and other types of suspended matter decrease WLR. Spectral variations of ocean reflectance are accounted for in a climatological sense using a wavelength dependent surface reflectance data set. Short-term variability, however, is not taken into account in the current version of the algorithm. Ocean retrievals of AOD and AAOD are not reported for sun glint angles smaller than 40º. The UV aerosol index is not reported for sun glint angles less than 20º.

The AOD over land is expected to have the same root mean square (RMS) error as TOMS retrievals (0.1 or 30% whichever is larger). The RMS error in AOD over water is likely to be 2 times larger. The RMS error for AAOD is estimated to be ~0.01.

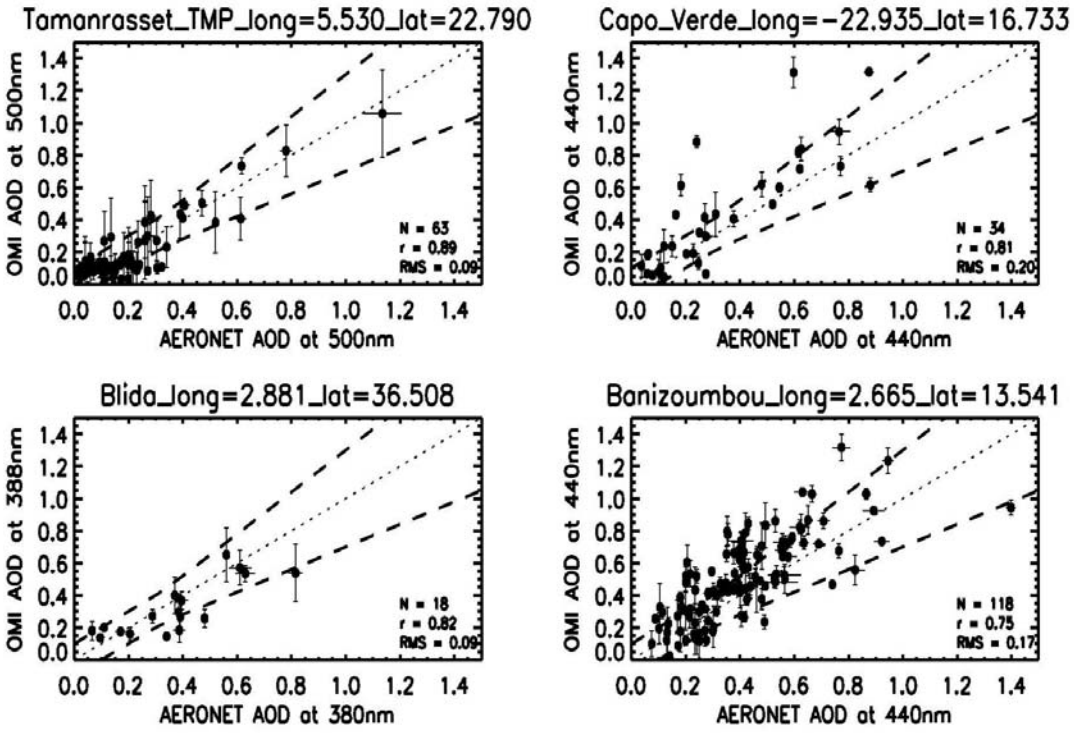

Figure 11. OMI-AERONET comparison over Northern Africa. At the Capo-verde and Banizombou sites OMI AOD retrievals have been reduced to 440 nm to facilitate the comparison.

Preliminary comparisons of OMAERUV-retrieved optical depth to AERONET observations at several sites show that when cloud-free conditions prevail OMAERUV-observed AOD values are in reasonable agreement with AERONET. Figure 2 illustrates a comparison of OMIAERUV retrieved AOD to AERONET measurements at four Northern Africa sites, where the atmospheric aerosol load typically consists of desert dust. The level of agreement is very good with correlation coefficients between 0.75 and 0.89.

For environments where sub-pixel cloud contamination is persistent during all seasons the statistics of the OMAERUV-AERONET comparisons are poor. For these conditions comparisons over a longer period are needed to better assess the quality of the OMI aerosol product.

As part of the data quality assessment OMAERUV retrievals of AOD have been compared to MODIS data for different aerosol types. In general, when clear conditions predominate, the OMAERUV and MODIS AOD products are well correlated, especially for large-scale dust and smoke events. For background aerosol conditions, sub-pixel cloud contamination significantly affects the OMI retrieval.

A comparison of OMAERUV AOD retrievals to airborne AOD observations by the AMES Airborne Tracking Sun-photometer (AATS-14) during the MILAGRO/INTEX-B field campaign was carried out. Most collocated measurements corresponded to oceanic background conditions. In general, the collection 2 OMAERUV retrieved AOD was significantly larger than the AATS-14 observation. The comparison using OMAERUV collection 3 data shows significant improvement. Users are strongly advised to consult with the OMI Quality Assurance Team for most recent information on our ongoing assessment of OMAERUV data quality.

4.3.2 Additional Information

For questions and comments related to the OMAERUV algorithm and data quality, please contact Omar Torres (omar.torres@hamptonu.edu) who has the overall responsibility for this product.

For more information on this product, refer to
http://disc.gsfc.nasa.gov/Aura/OMI/omaeruv_v003.shtml.

4.4 OMI/Aura Bromine Monoxide Total Column (OMBRO)

4.4.1 Quality Assessment

Fitting uncertainties for the BrO slant columns (single measurement) typically range between 25-100% , with as low as 5% over BrO hotspots. This is roughly 2-4 times what was achieved from GOME. Uncertainties in the stratospheric air mass factor (AMF), used to convert slant to vertical columns, are estimated to be 10% or less. Hence the total uncertainties of the BrO vertical columns typically range within 27-101%.

Across-track striping (systematically elevated or reduced column values at the same cross track position along the whole track) of the BrO columns is still an issue, despite the improvements achieved in OMBRO v2.0 (Collection/Product Version 003). This is not unique to BrO but affects all OMI data products to a greater or lesser extent. Small absorbers like BrO, HCHO and OClO however, are more strongly affected by striping since the column values are of a similar order of magnitude as the stripes, so that the effect is relatively stronger. Users of the BrO columns provided here must be aware of this issue.

The BrO data product provides RMS (data field *FittingRMS*) and one standard deviation (1σ) fitting uncertainties (*ColumnUncertainty*), as derived from the fitting covariance matrix. The uncertainties do not include contributions from uncertainties in the measurements or the reference cross sections. The main guidance to data quality provided with the BrO columns is the *MainDataQualityFlag*, which is set to any of four values (0, 1, 2, and -1) based on the outcome of the fitting process (see description below, under "Which Data Should Be Used?"). This flag should be used for data screening prior to use of each individual OMI pixel column. Additional information on the convergence of the fit is provided in a fitting diagnostic flag (*FitConvergenceFlag*); this flag should be consulted if more detailed information on the fitting process is desired.

Table 10: Which Data Should be Used

Value	Classification	Rationale
0	Good	Column value present and passes all quality checks; data may be used with confidence.
1	Suspect	Caution advised because one or more of the following conditions are present: • *FitConvergenceFlag* is < 300 (but > 0): convergence at noise level • Column+2σ uncertainty < 0 (but Column+3σ uncertainty ≥ 0) • Absolute column value > *MaximumColumnAmount* ($1 \cdot 10^{19}$ mol/cm^2)
2	Bad	Avoid using data because one or more of the following conditions are present: • *FitConvergenceFlag* is < 0: abnormal termination, no convergence • Column+3σ uncertainty < 0
≤ -1	Missing	No column values have been computed; entries are missing

4.4.2 Additional Information

For questions and comments related to the OMBRO algorithm and data quality, please contact Thomas P. Kurosu (tkurosu@cfa.harvard.edu). Please send a copy of your e-mail to Kelly Chance (kchance@cfa.harvard.edu), who has the overall responsibility for this product.

For more information on this product, refer to
http://www.cfa.harvard.edu/~tkurosu/SatelliteInstruments/OMI/PGEReleases/index.html
and
http://www.cfa.harvard.edu/~tkurosu/SatelliteInstruments/OMI/PGEReleases/READMEs/OMBRO_README.pdf

4.5 OMI/Aura Cloud Pressure and Fraction (O_2-O_2 Absorption) (OMCLDO2)

4.5.1 Quality Assessment

The OMCLDO2 effective cloud fraction and cloud pressure have been compared to MODIS Aqua, which flies 15 minutes in front of OMI. This comparison is described in the proceeding (PDF) for the ESA Atmos Conference (Frascati, 9-12 May 2006) and in the Journal of Geophysical Research (P. Stammes, M. Sneep, J.F. de Haan, J.P. Veefkind, P. Wang and P.F. Levelt, Effective cloud fractions from the Ozone Monitoring Instrument: Theoretical framework and validation, J. Geophys. Res., 2008, 113, doi:10.1029/2007JD008820). The most important conclusions are:

1. The effective cloud fraction of OMI compares well to an effective cloud fraction derived from MODIS' cloud optical thickness. Large differences may occur of snow and ice surfaces. Also, the OMI cloud fractions are slightly higher at low effective cloud fractions.

2. The cloud top pressure derived from MODIS is lower (higher clouds) than OMI. This is expected because MODIS uses the thermal infrared, which is more sensitive to higher clouds. The bias between OMI and MODIS is approximately 100 hPa, with a standard deviation of 200 hPa. It is noted that the comparison of the cloud pressure is difficult because of the different wavelength regions.

Further investigations on the accuracy of the OMCLDO2 product are published in the Journal of Geophysical Research (M. Sneep, J.F. de Haan, P. Stammes, P. Wang, C. Vanbauce, J. Joiner, A.P. Vasilkov and P.F. Levelt, Three way comparison between OMI and PARASOL cloud pressure products, J. Geophys. Res., 2008, 113, doi:10.1029/2007JD008694, including a limited comparison with the CloudSat space borne cloud radar.

Row Anomalies

Several "row anomalies" have occurred in the recent past. These anomalies affect the quality of the Level 2 data products, including OMCLDO2. Each download site for OMI data contains a warning on which rows are affected by these anomalies, and the starting date for each event. Please note that rows that are not listed are unaffected, and of optimal quality.

Please be aware that these anomalies are known to the OMI team and are currently under investigation. The detailed technical information page describes the effect on the OMI spectra. The release details document describes the effect of the anomaly and corrections that are implemented in OMCLDO2 itself in more detail.

4.5.2 Additional Information

Questions related to the OMCLDO2 dataset should be directed to the GES DISC at help-disc@listserv.gsfc.nasa.gov. For questions and comments related to the OMCLDO2 algorithm and data quality please send mail to contact omcldo2@ltpmail.gsfc.nasa.gov.

For more information on this product, refer to:
http://disc.gsfc.nasa.gov/Aura/OMI/omcldo2_v003.shtml

4.6 OMI/Aura Cloud Pressure and Fraction (Raman Scattering) (OMCLDRR)

4.6.1 Quality Assessment

When accessing data quality, be aware that both the OMCLDRR cloud pressure and fraction are "effective," meaning that the cloud fraction does not represent true geometrical cloud fraction and the cloud pressure may not represent the true physical cloud-top pressure (especially in the case of multiple cloud layers). Specifically, it is difficult to derive a sub-pixel cloud fraction using OMI radiances. The effective cloud fraction is based on gross assumptions about the cloud and ground reflectivities. The effective cloud fraction is intended for use in conjunction with the effective cloud pressure such that the combination of the two produces the amount of observed Raman scattering.

The cloud pressures are representative of pressure levels reached by back-scattered photons averaged over a weighting function. The algorithm uses the concept of the Mixed Lambertian-Equivalent Reflectivity (MLER) in which a surface (cloud or ground) is assumed opaque and Lambertian. In the MLER model, a cloud fraction is used to weight the radiances coming from the clear and cloudy portions of the pixel. The algorithm computes an effective cloud fraction using assumptions about the cloud and ground reflectivities as will be described below. Scattering and/or absorption from within and below a cloud or between multiple cloud decks can be accounted for by using a pressure higher than the physical cloud top. The derived effective cloud pressures are therefore typically higher than (that is, lower in altitude) cloud-top pressures such as those derived from thermal infrared measurements and cloud lidars. Based on preliminary comparisons with MODIS, we find the effective cloud pressures (CloudPressure) to be on average about 250 hPa higher than the physical cloud-top. These numbers are consistent with previous studies using different instruments (for example, GOME/ATSR).

The original (pre-launch) estimates of the accuracy and precision of the effective cloud pressure retrieval were 100 and 30 hPa, respectively. Preliminary comparisons with MODIS (Joiner, et al., 2004; Vasilkov et al., 2004; Joiner and Vasilkov, 2006; Vasilkov et al., 2008) and the Cloud Physics Lidar (CPL) (Joiner et al., 2006) and more recently

with CloudSat (Vasilkov et al., 2008) are consistent with radiative transfer calculations that show enhancement in scattering from multiple cloud decks (which may occur frequently) and significant light penetration into physically thick clouds, especially deep convective clouds. Based on these comparisons and considerations, we believe that our original error estimates are reasonable for optically thick clouds ($\tau > 20$) and for lower τ at Solar Zenith Angles (SZA) near 45 degrees. However, at lower τ and higher and lower SZA, the retrieved cloud pressures may have significant errors, but they should still be sufficiently accurate for use in trace gas retrievals.

4.6.1.1 Algorithm Quality Assessment

1. In Version 1.0 of OMCLDRR, we used the spectral range 392-398 nm. We found that this fitting window had some undesirable features including (1) sensitivity to Raman scattering in the ocean, (2) significant sensitivity to non-Lambertian behavior of clouds and ground including cloud shadowing, thin cloud phase function, and non-Lambertian behavior of the surface (for example, sea glint), and (3) problems with the MLER model in the presence of thin/broken clouds that produced too low and sometimes negative cloud pressures. In Version 1.1 and beyond, we use the fitting window 346-354 nm. There is significantly more Rayleigh scattering at these wavelengths that mitigates–but does not completely eliminate–problems associated with all of the features mentioned above. Due to the change in the fitting window, OMCLDRR now uses the UV-2 channel to derive cloud pressure, cloud fraction, and reflectivity. This has an added benefit that the cloud fields will have slightly better co-registration with other OMI products (ozone, BrO, and HCHO) that use the UV-2 channel.
2. Under low cloud fraction conditions (< ~0.3), sea glint can cause erroneously high values of retrieved reflectivity and low values of cloud pressure. Sea glint primarily affects the west side of a swath at low and mid-latitudes. The sea glint possibility flag is contained in bit 4 of the ground pixel quality flag. As mentioned above, cloud pressures are much improved in v1.1 over sea glint conditions.
3. Over snow/ice, the processing quality flag bit 5 is set to 1, and the cloud fraction is assigned to 1. Therefore, the effective cloud pressure for these pixels is representative of an average scene pressure (that is, the LER pressure of a pixel that produces the observed amount of Raman scattering). This is done for a more positive identification of the existence of thick clouds over snow/ice. This is of interest for the retrieval of ozone and other trace gases as well as the calculation of surface UVB. The snow/ice information comes from the Near real-time Ice and Snow Extent (NISE) product created using passive microwave data. It is provided by the National Snow and Ice Data Center (NSIDC) and is included in the Level 1b data set.
4. As the cloud fraction tends to zero, the error in retrieved cloud pressure increases rapidly. These errors can occur in some cases where cloud fractions are very low (approaching 20%). Therefore, for cloud fractions < 5%, we do not attempt a

cloud pressure retrieval. Instead, an effective scene pressure is reported for diagnostic purposes only. These cases are indicated where bit 13 of the processing quality flag is set to 1. Retrievals for cloud fractions < 20% are considered to be suspect and should be used with caution.

5. Transient events due to radiation hits on a detector may produce striping in the cloud pressures (for example, anomalously low or high values at one scan position). This may last only for a short period or may continue until elevated dark currents are adjusted in the calibration; these adjustments are made daily in Collection 3. Transient data are currently flagged in the Level 1b data set. OMCLDRR has the option of checking this flag. However, the default is currently not to check the flag. When the transient flag is checked, the algorithm disregards affected transient pixels as well as pixels affected by other types of errors within the fitting window. In practice, we found that the transient flags are set very infrequently and our internal quality control checks are able to detect affected pixels most of the time. When any type of warning or error occurs for pixels within the fitting window for radiance or irradiances, bits 9-12 of the processing quality flag are set as appropriate.
6. Absorbing aerosol in and above clouds can affect the OMCLDRR data. In general, it will reduce the cloud fraction and pressures. The presence of absorbing aerosols is currently not flagged in the OMCLDRR file. The aerosol index flag in the OMTO3 file can be used to check for the existence of absorbing aerosol within a pixel.
7. Version 1.4 uses a surface albedo climatology based on TOMS. Previous versions assumed a surface reflectivity of 15% consistent with OMTO3. With this change and additional changes in the instrument calibration in Collection 3, we find the cloud pressures to be higher on average than in previous versions, particularly at low cloud fractions.

4.6.2 Additional Information

Questions related to the OMCLDRR dataset should be directed to the GES DISC at help-disc@listserv.gsfc.nasa.gov. Users interested in these parameters, or having other questions regarding the OMCLDRR dataset, are advised to contact Alexander Vasilkov (alexander_vassilkov@ssaihq.com) and Joanna Joiner (Joanna.Joiner@nasa.gov), who has the overall responsibility for this product.

For more information on this product, refer to:
http://disc.gsfc.nasa.gov/Aura/OMI/omcldrr_v003.shtml
http://acdb-ext.gsfc.nasa.gov/People/Joiner/OMCLDRR_README.htm
http://acdb-ext.gsfc.nasa.gov/People/Joiner/OMCLDRR_validation_web.htm
http://acdb-ext.gsfc.nasa.gov/People/Joiner/OMCLDRR.fs

4.7 OMI/Aura DOAS Total Column Ozone (OMDOAO3)

4.7.1 Quality Assessment

The release specific information about OMDOAO3 contains details on specific features and problems in the data product and this document should be read before using the data.

The OMI project team uses two total ozone (O3) retrieval algorithms, OMI-TOMS and OMI-DOAS, in order to maintain the long term TOMS data record as well as to improve the ozone column estimate using the hyperspectral capability of OMI. Kroon *et al.* (J. Geophys. Res., 2008, 113, D16S28, doi:10.1029/2007JD008798) assessed where the algorithms produce comparable results and where the differences are significant. Mean differences in the two ozone column estimates vary from 0-9 DU (0-3%), and their correlation coefficients vary between 0.89 and 0.99 with latitude and season. The largest differences occur in the Polar regions and over clouds. These differences have been exemplified by comparisons of OMI satellite data with AVE airborne data in the paper by Kroon *et al.* (J. Geophys. Res., 2008, 113, D15S13, doi:10.1029/2007JD008795). Continuing the TOMS total ozone column data record that dates back to November 1978 is the primary OMI mission goal that is achievable with either OMI total ozone column data product.

The paper by Balis *et al.* (J. Geophys. Res., 2007, 112, D24S46, doi:10.1029/2007JD008796) present the validation of the OMI total ozone column data products through comparisons with quality controlled and archived data from ground-based observations by Dobson and Brewer spectrophotometer instruments located at stations worldwide. The study focused on global comparisons and seasonal dependence, and the possible dependence on latitude and solar zenith angle. The results show a globally averaged agreement of better than 1% for OMI-TOMS data and better than 2% for OMI-DOAS data with the ground-based observations. The OMI-TOMS data product is shown to be of high overall quality with no significant dependence on solar zenith angle or latitude. The OMI-DOAS data product shows no significant dependence on latitude except for the high latitudes of the Southern Hemisphere where it systematically overestimates the total ozone value. In addition a significant dependence on solar zenith angle is found between OMI-DOAS and ground-based data.

Ground-based observations with a Fourier transform spectrometer in the infrared region (FTIR) were performed in Kiev (Ukraine) during the time frames August-October 2005 and June-October 2006 by Shavrina *et al.* (J. Geophys. Res., 2007, 112, D24S45, doi:10.1029/2007JD008787). FTIR based estimates of ozone columns from the 2006 observations compare rather well with the OMI total ozone column data: standard errors are of 1.11 DU and 0.68 DU, standard deviation are of 8.77 DU and 5.37 DU for OMI DOAS and OMI TOMS, respectively.

The overview paper by McPeters *et al.* (J. Geophys. Res., 2008, 113, D15S14,

doi:10.1029/2007JD008802) summarized these and other validation exercises for the OMI total ozone column data products.

To assess the quality of individual retrievals it is very important to look at the quality flags fields in the data products, as described in the Product Format Specification. Especially the ProcessingQualityFlags are important to filter for bad quality data. The best quality data have a ProcesingQualityFlags of 0. It is recommended to apply a bitwise AND on the ProcessingQualityFlags field using a value of 43679 to filter the data. This will filter all data for which the ProcessingQualityFlags bits 0, 1, 2, 3, 4, 7, 9, 11, 13 and/or 15 are set.

4.7.2 Additional Information

Questions related to the OMDOAO3 dataset should be directed to the GES DISC. For questions and comments related to the OMDOAO3 algorithm and data quality, please contact omdoao3@ltpmail.gsfc.nasa.gov.

For more information on this product refer to:
http://disc.sci.gsfc.nasa.gov/Aura/OMI/omdoao3_v003.shtml

4.8 OMI/Aura Formaldehyde (HCHO) Total Column (OMHCHO)

4.8.1 Quality Assessment

Fitting uncertainties for the HCHO slant columns (single measurement) typically range between 40-100% , with the lower end of this range over HCHO hotspots. This is roughly comparable to what has been achieved from GOME. Uncertainties in the air mass factor (AMF), used to convert slant to vertical columns, are estimated to be 30%. Hence the total uncertainties of the HCHO vertical columns typically range within 50-105%.

Other quality issues remain the same as for BrO (OMBRO).

4.8.2 Additional Information

For questions and comments related to the OMHCHO algorithm and data quality, please contact Thomas P. Kurosu (tkurosu@cfa.harvard.edu). Please send a copy of your e-mail to Kelly Chance (kchance@cfa.harvard.edu), who has the overall responsibility for this product.

For more information on this product, refer to:
http://www.cfa.harvard.edu/~tkurosu/SatelliteInstruments/OMI/PGEReleases/README s/OMHCHO_README.pdf

4.9 OMI/Aura Nitrogen Dioxide (NO2) Total and Tropospheric Column (OMNO2)

4.9.1 Quality Assessment

The quality of the data in this release is currently being established by independent measurements in ongoing validation campaigns from ground-, aircraft-, and satellite-based instruments. An overview of the validation results to date are presented in Celarier, et al., (2008). The principal findings from those validation efforts are summarized in the following table.

Data quality issues are described in the Data Quality document found at
http://toms.gsfc.nasa.gov/omi/no2/OMNO2_data_quality.pdf.

An overview of some of the validation efforts may be found in the presentation
http://earth.esa.int/workshops/atmos2006/participants/330/pres_330_kroon.pdf.

Stratospheric amounts are in reasonable agreement with climatological measurements from the Halogen Occultation Experiment (HALOE) instrument aboard the Upper Atmosphere Research Satellite (UARS) and with model calculations from the NASA/GSFC chemical transport model (CTM). Tropospheric amounts are generally consistent with the GEOS-CHEM model and indicate prominent sources near urban areas.

The data product includes estimates of uncertainties associated with the various geophysical quantities. The uncertainty estimates have been improved since the provisional release of the OMI data. However, these estimates may not account for all actual sources of random or systematic errors. We anticipate further improvements through the validation process and in understanding the probability distributions of the underlying data and the algorithmic sensitivity to the data.

4.9.2 Additional Information

For questions and comments related to the OMNO2 algorithm and data quality, please contact omno2@ltpmail.gsfc.nasa.gov. Additional questions may be directed to the principal points of contact for OMNO2:
James F. Gleason (James.F.Gleaon@nasa.gov) and
J. Pepijn Veefkind (veefkind@knmi.nl).

For more information on this product, refer to:
http://toms.gsfc.nasa.gov/omi/no2/OMNO2_readme.pdf
http://toms.gsfc.nasa.gov/omi/no2/OMNO2_release_notes.pdf
http://toms.gsfc.nasa.gov/omi/no2/OMNO2_data_quality.pdf
http://toms.gsfc.nasa.gov/omi/no2/OMNO2_data_product_specification.pdf

4.10 OMI/Aura Ozone Profile (OMO3PR)

4.10.1 Quality Assessment

The OMO3PR data have been assessed using MLS stratospheric ozone profiles and OMDOAO3 total ozone data. The tropospheric information has not been validated. *It is recommended to be extremely cautious with any conclusions on tropospheric ozone based on these data.*

Comparison with MLS

A comparison of the OMO3PR with MLS stratospheric ozone profile data can be found in a separate document. Figure 2 shows an example of comparisons with MLS for August 1, 2007.The main conclusions of these comparisons are:

1. Overall the OMO3PR optimal estimation results are as expected from simulated results. The averaging kernels are well behaved in the stratosphere. In the troposphere the averaging kernels are broad and approximately one piece of independent information is available for the troposphere. In the upper troposphere and lower stratosphere little profile information is contained in the UV spectrum.
2. Comparison with MLS for the pressure range up to 400 hPa (cf. Figure 12) show that the OMO3PR results agree very well with the MLS profiles. There remain some oscillations in the differences between the profiles, but the amplitude of these oscillations is reduced significantly compared to previous versions of OMO3PR, mainly due to the fitting of stray light and a change in the a-priori climatology. Relatively large differences occur for pressures of 100 – 200 hPa in the southern hemisphere, possibly due to differences in the a-priori climatology. The OMO3PR and MLS integrated ozone columns from the TOA until 300 hPa agree within a few percent.
3. The results presented in this document focus on the stratospheric profile and the total column. The tropospheric sub-column has not been evaluated.

Performance for Ozone Hole Conditions

In version 1.0.5 the Gasuss-Newton iteration method was used which converges very slowly if the a-priori differs strongly from the true profile, as happens often during ozone hole conditions. In version 1.1.0 a modified Levenberg-Marquardt iteration scheme is used which converges much faster when the a-priori differs strongly from the true profile. This led to a considerable improvement of the performance during ozone hole conditions.

Performance over Absorbing Aerosol Layers

Over elevated absorbing aerosol layers the ozone profile retrieval will put too much ozone in the troposphere. Therefore it is not recommend using these data. The absorbing aerosol index can be used to identify such absorbing aerosol layers.

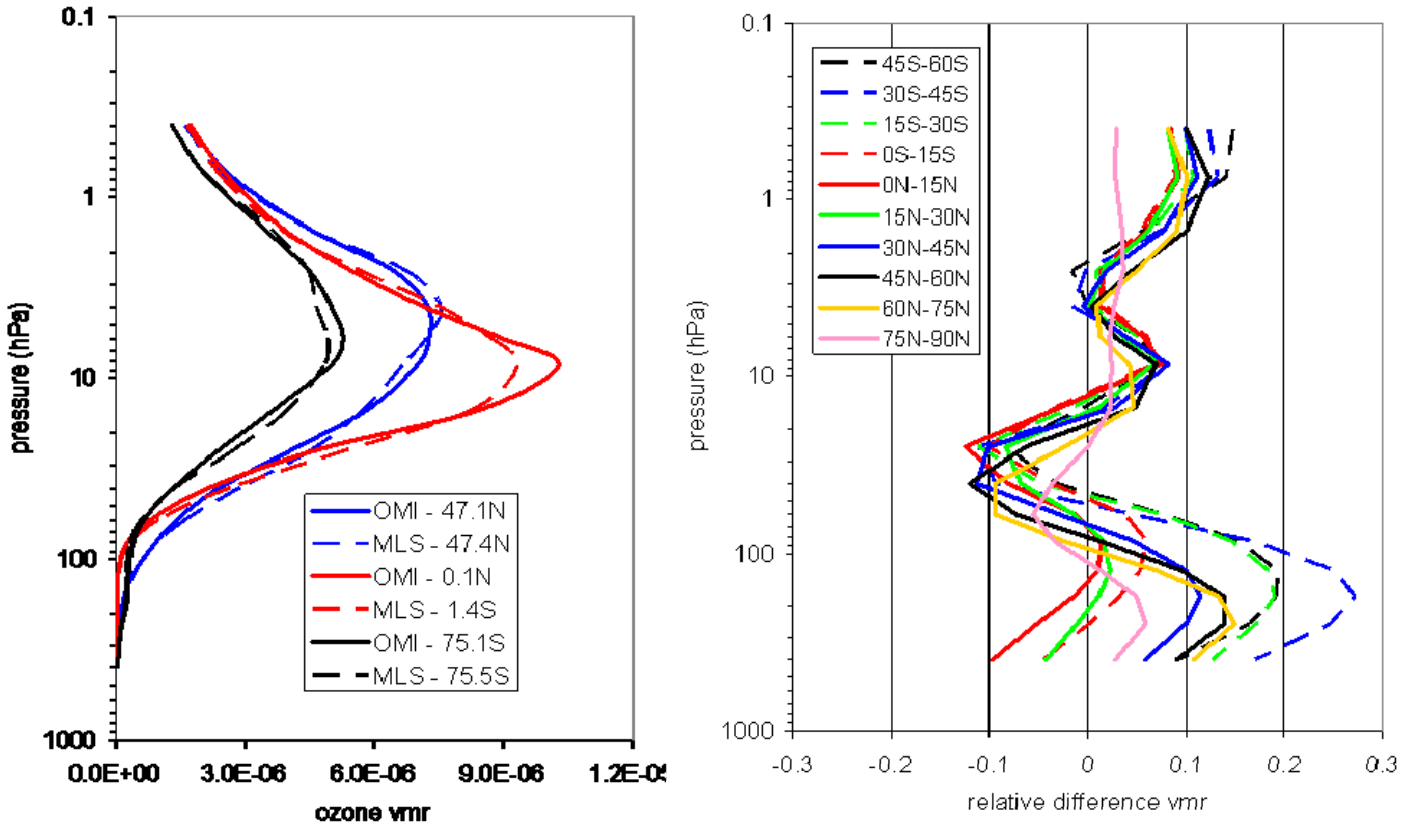

Figure 12. Left: Comparison of retrieved profiles from OMI (solid) and MLS (dashed) for three latitudes for OMI orbit 6754 in week 42 2005. The black curves pertain to a part of the ozone hole. The latitudes used are listed in the legend. Right: Average relative differences between ozone profile retrieved from OMI and MLS for week 30 2005 (OMI orbits 5428 – 5529). Results are given for different latitude bands and solid lines are for the northern hemisphere while dashed lines are for the southern hemisphere. For each latitude band about 2000 co-locations were used, except for 45S-60S where 681 co-locations were used.

OMI Row Anomaly

Three recent anomalies (first starting June 25 2007, second starting May 11 2008, and third starting January 24 2009) have been observed in the OMI Measurements. The anomalies are currently under investigation. **Until further notice, the OMO3PR**

product should not be used after the start of the first anomaly. After the investigation is finished it will be made clear what part of the data after June 25, 2007 can be used.

4.10.2 Additional Information

For questions related to the OMO3PR dataset please contact help-disc@listserv.gsfc.nasa.gov. For questions and comments related to the OMO3PR algorithm and data quality please contact omo3pr@ltpmail.gsfc.nasa.gov.

For more information on this product, refer to:
http://disc.sci.gsfc.nasa.gov/Aura/data-holdings/OMI/omo3pr_v003.shtml

4.11 OMI/Aura Chlorine Dioxide Slant Column (OMOCLO)

4.11.1 Quality Assessment

Fitting uncertainties for the OClO slant columns (single measurement) typically range between 40-100% , with the lower end of this range within the Antarctic polar vortex where OClO is most abundant. More details on algorithm specifics can be found in the *OMI Algorithm Theoretical Basis Document*, Volume 4, and in Kurosu et al., 2004.

Other quality issues remain the same as for BrO (OMBRO).

4.11.2 Additional Information

For questions and comments related to the OMOCLO algorithm and data quality, please contact Thomas P. Kurosu (tkurosu@cfa.harvard.edu). Please send a copy of your e-mail to Kelly Chance (kchance@cfa.harvard.edu), who has the overall responsibility for this product.

For more information on this product, refer to:
http://www.cfa.harvard.edu/~tkurosu/SatelliteInstruments/OMI/PGEReleases/README s/OMOCLO_README.pdf

4.12 OMI/Aura Sulfur Dioxide Total Column (OMSO2)

4.12.1 Quality Assessment

The accuracy and precision of the derived SO2 columns vary significantly with the SO2 CMA (Center of Mass Altitude) and column amount, observational geometry, and slant column ozone (Krotkov et al 2006; 2008; Yang et al., 2007). Separate Quality Flags (QFs) are provided for each of the 4 SO2 products, corresponding to different sources: fossil fuel combustion, smelters, volcanic degassing, and volcanic eruptions. However, analysis of the QF values has shown that they work best for strong volcanic plumes, but reject pollution and low level degassing emissions. **When averaging SO2 data users are**

advised not using QF. Below are data quality assessments for each SO2 **ignoring QFs**:

1) ColumnAmountSO2_PBL: **Due to reduced OMI sensitivity to SO2 in PBL this product should be used only under optimal viewing conditions: cloud fraction <0.2, solar zenith angle < 50o and near-nadir viewing angles (cross track positions 10 to 50). Precision:** The noise standard deviation (sigma) is ~1.2DU-1.5 DU in the tropics, but increases with latitude, viewing and solar zenith angles and total ozone. Given this large noise only plumes from strong anthropogenic sources of SO2 (such as smelters and coal burning power plants) and from strong regional pollution can be detected in scene data (Carn et al 2007a; Krotkov et al 2008). Averaging over a larger area or for a longer time reduces the noise but slower than the square root of the number of scenes averaged. The standard deviation reduces to ~0.8 DU when 4 scenes are averaged and approaches ~0.4 DU with increasing number of averaged scenes. The SO2 detection limit is roughly twice of the 1sigma noise.

Accuracy: The SO2 retrieval accuracy depends on the uncertainty in both *SCD* (slant column density) and in average photon path, characterized by the error in assumed air-mass factor (*AMF*). The *AMF* error is systematic and increases with deviation of the observational conditions from those assumed in the operational algorithm. For cloud-free scenes, the *AMF* can be corrected using OMI slant column ozone (*SCO*) data as described in Krotkov et al (2008). For large *SCO* values >1500 DU (i.e. high ozone and/or high solar zenith and viewing angles, mostly at high latitudes), the *AMF* becomes very small, so valid PBL SO2 retrievals are not expected. In addition, aerosols and sub pixel clouds affect the *AMF* in different ways depending on their vertical distribution. Though clouds screen PBL SO2, we have not attempted to correct for this effect. For this reason we do not recommend using this product when the radiative cloud fraction (RCF) exceeds 0.2.

2) ColumnAmountSO2_TRL: Due to increased sensitivity to elevated SO2, the 1 sigma noise in TRL data is reduced to ~0.7 DU under optimal observational conditions in the tropics. The data can be used for cloudy, clear and mixed scenes as well as for elevated terrain. However, the TRL data contain filled values when terrain pressure or OMCLDRR effective cloud pressure is less than ~500hPa. In such cases the cloud blocks most of the SO2. As a result, the SO2 weighting function approaches zero, no LF retrieval is done and the fill value is stored in the output.

3) ColumnAmountSO2_TRM: This product is optimized for typical volcanic degassing from volcanoes with vents at ~5km altitude or above and emissions from effusive eruptions. The standard deviation of TRM retrievals in background areas is about 0.3 DU at low and mid-latitudes. The cloud-related fill values in TRM data occurs only when the OMI measured cloud top is higher than ~8-10 km. Biases in the TRM retrievals due to latitude and viewing angle are removed to the 0.1 DU level by the median residual background corrections. Both the bias and standard deviations increase with solar zenith angle. **We recommend that the TRM retrievals be used for volcanic degassing cases at all altitudes** because the PBL retrievals are restricted to optimal viewing conditions and TRL data are overestimated for high altitude emissions (>3km). In general, SO2

releases at altitudes less than ~7.5 km will be underestimated, but these errors can be corrected off-line using the averaging kernel Yang et al (2007) if the actual SO2 vertical distribution is known. Analysis of daily OMSO2 data for degassing volcanoes at high altitude (~5 km) has shown that significant trends in SO2 burdens, linked to variability of source SO2 emissions, can be detected (Carn et al., 2008). Preliminary surveys of global volcanic OMSO2 data indicate that the current sensitivity of the algorithm permits detection of volcanoes emitting on the order of 1000 tons SO2/day or more in daily data (under optimal viewing conditions). Detection of weaker sources usually requires temporal averaging of the OMSO2 data.

4) ColumnAmountSO2_STL data are intended for use with explosive volcanic eruptions where the cloud is placed in the upper troposphere or stratosphere (UTLS). At these altitudes the averaging kernel is weakly dependent on altitude, so that differences in actual cloud height from ~17 km produce only small errors. The biases with latitude and viewing angle are generally less than 0.2 DU. The noise level in background data is about 0.2 DU. This sensitivity has permitted tracking of volcanic SO2 clouds in the UTLS for great distances from the source (e.g., Carn et al., 2007b, Carn et al., 2009). Both the bias and standard deviation increase near the northern terminator, similar to but reduced from the TRM results. Artifacts due to ozone profile errors are reduced from the TRM data by about 30%. One should see no fill values due to cloud screening in the STL data. The LF algorithm as implemented in the v1.1.1 OMSO2 is expected to provide good retrieval when SO2 loading is less than ~50 DU. When SO2 loadings are higher than ~100 DU the LF algorithm underestimates the true SO2 amount, the higher the loading the larger the underestimation (Yang et al 2007; Yang et al., 2009). Comparisons between total SO2 burdens calculated using OMSO2 and EP-TOMS SO2 data for volcanic clouds in the UTLS have shown agreement to within 20% for SO_2 column amounts of <100 DU.

4.12.2 Additional Information

Several articles are published about OMSO2 products (Carn et al, 2007a; Carn et al, 2007b; Krotkov et al., 2007; Yang et al., 2007; Krotkov et al., 2008; Yang et al., 2009).

For questions and comments related to the OMSO2 algorithm and data quality, contact Nickolay Krotkov (Nickolay.A.Krotkov@nasa.gov)who has the overall responsibility for this product and send copies to Kai Yang (Kai.Yang.1@nasa.gov).

For more information on this product, refer to:
http://so2.umbc.edu/omi/Documentation/OMSO2Readme_V111_0818.htm.

4.13 OMI/Aura Ozone (O_3) Total Column (OMTO3)

4.13.1 Quality Assessment

Overall the quality of total ozone and AI data produced by OMTO3 is similar to that from TOMS (http://toms.gsfc.nasa.gov/), except for cloudy observations. Based on experience

with TOMS, the total ozone data provided in OMTO3 should have a root-mean squared error of 1-2%, depending on solar zenith angle, aerosol amount, and cloud cover. These errors are best described as pseudo-random: systematic over small areas with a unique geophysical regime, random over large areas containing a mixture of geophysical regimes. Preliminary analyses show that OMTO3 data compare about as well with Dobson and Brewer stations as did Nimbus-7/TOMS data. (The overall quality of EP/TOMS data is poorer compared to both Nimbus-7 TOMS and OMI. The EP/TOMS total ozone data have been reprocessed recently by applying an empirical correction, developed using NOAA/SBUV-2 data, to remove several poorly understood instrument anomalies. The AI data from EP/TOMS, however, have not yet been corrected.)

4.13.2 Additional Information

For questions and comments related to the OMTO3 algorithm and data quality, please contact Kai Yang (Kai.Yang-1@nasa.gov). Please send a copy of your e-mail to P.K. Bhartia (pawan.bhartia@nasa.gov), who has the overall responsibility for this product.

For more information on this product, refer to:
http://toms.gsfc.nasa.gov/omi/OMTO3Readme.html
http://disc.gsfc.nasa.gov/Aura/OMI/omto3_v003.shtml

4.14 OMI/Aura Surface UV Irradiances (OMUVB)

4.14.1 Quality Assessment

The radiative transfer model assumes that clouds are plane parallel and homogeneous, i.e., it doesn't account for broken, multi-layer or mixed phase clouds. This error is the principal source of noise in comparing satellite measurements with ground-based instruments. The OMI surface UV irradiance represents the spatial average over the OMI footprint. OMI measurements are made once a day around 1:45 p.m. local time. No correction is made for the change in cloudiness, ozone and aerosols between local noon and satellite overpass time, or for their diurnal variability. Previous validation studies with TOMS data suggest that OMI UV irradiance estimates are on the average 0-30% larger than the ground-based reference data. The OMI surface UV data were compared with spectral ground-based measurement data of several stations, e.g. Jokioinen (60.8N,23.5E), Sodankyla (67.4N,26.6E), Toronto (43.8N,79.5W), San Diego (32.8N,117.2W), Ushuaia (54.8S,68.3W), and Barrow (71.3N,156.7W). The validation results of Tanskanen et al. 2007 imply similar results as the previous validation studies with TOMS surface UV data. The systematic bias can be attributed to absorbing aerosols from natural and anthropogenic sources. Since the soot content of the urban aerosols tend to be highly localized, these errors presumably are also localized and do not necessarily represent the error in regional estimate of surface UV made by OMI. Snow and ice further complicate estimation of the surface UV since clouds cannot be distinguished from them. Therefore, in regions with temporary snow or ice or highly heterogeneous surface albedo the OMI UV irradiance estimates have much higher uncertainty. Future

version of the algorithm may use snow cover information to reduce this uncertainty.

4.14.2 Additional Information

Questions and comments related to the OMUVB dataset, the OMI Surface UV algorithm, or data quality should be directed to Antti Arola (antti.arola@fmi.fi).

For more information on this product, refer to
http://disc.gsfc.nasa.gov/Aura/OMI/omuvb_v003.shtml.

4.15 Important Information for OMI Data Users

4.15.1 Row Anomalies

Several row anomalies have occurred in the recent past. These anomalies affect the quality of the Level 1B and Level 2 data products. Please read this information carefully prior to using OMI data. Please respect the dates mentioned as the anomalies have occurred recently. Our detailed technical information is available at: http://www.knmi.nl/omi/research/product/rowanomaly-background.php. Please visit this page for more information.

Table 11: Cross-Track Anomalies

Anomaly	Date since its occurrence	Affected cross-track positions (0-based)
Anomaly 1	Since June 25th, 2007	53-54
Anomaly 1	Since May 11th, 2008	37-44
Anomaly 1	Since January 24th, 2009	27-44

Please be aware that for all other rows of the data are of optimal quality and not affected. Also all OMI data before these anomalies are of optimal quality.

4.15.2 Row Anomaly Corrections

Please be aware that these anomalies are known to the OMI team and are currently under investigation to examine whether corrections for the effects can be implemented in the Level 1b data. Please visit this information page regularly for updates on the status of corrections implemented and visit our detailed technical information page at the above address.

4.15.3 Row Anomaly Flagging

The Level 1B data are partially flagged for the anomalies listed above. Detailed technical information on the current flagging status of the Level 1B and Level 2 products is

available at http://www.knmi.nl/omi/research/product/rowanomaly-background.php

4.15.4 Recommendations to Users

At the moment no corrections have been implemented in the operational Level 1B and Level 2 data. It is recommended not to use the affected cross-track scenes.

Please respect the dates mentioned above. All other OMI data, meaning other cross track scenes and earlier observations, is of optimal quality. Level-3 products are being produced after filtering for the cross track scenes mentioned per anomaly.

Chapter 5: OMI Data Access and Use

5.1 Data Format

The majority of the datasets archived at the NASA's Goddard Earth Sciences Data and Information Services Center (GES DISC) are in the Hierarchical Data Format-Earth Observing System (HDF-EOS) format. NASA has adopted this format for standard data product distribution since it is able to handle multiple types of data objects and at the same time is independent of the platform or operating system the file has been created on.

Two versions of the HDF-EOS format, HDF-EOS 2.x (based on native HDF4 format) and HDF-EOS 5.x (based on native HDF5 format), are in use and are usually referred to as HE4 and HE5 format, respectively.

OMI Level 1B data files (radiances, irradiance, and calibration files) are written in HE4 format and OMI Level 2 and Level 3 products (derived geophysical parameters) are in HE5 format. The file names have the extension .he4 and .he5, respectively.

For tools to read HDF-EOS data files, please refer to "Section 5.3 Using OMI Data," Page 52 of this guide and to: http://disc.gsfc.nasa.gov/Aura/tools.shtml.

5.2 Accessing OMI Data

Publicly released Version 3 OMI Products are available from GES DISC home page at: http://disc.gsfc.nasa.gov/Aura/OMI/

OMI Level-2 data subsets for ground station overpass are available from Aura Validation Data Center link at http://avdc.gsfc.nasa.gov/index.php?site=2045907950.

Information about OMI data products is also available from KNMI web site at:

http://www.knmi.nl/omi/research/product/

5.3 Using OMI Data

Software and many tools have been developed by the NASA data centers and software developers to read HDF-EOS files. These tools examine and modify the HE4 and HE5 file contents, dump the files, extract the required data objects (images, orbital swath data, gridded data, and tables), display the content, convert files from old HDF format to new format and vice versa, and convert the file into familiar ASCII or binary format. Some of them are described below:

- **HDFview:** The HDFView is a visual tool for browsing and editing HDF4 and HDF5 files. Using HDFView, users can (1) view a file hierarchy in a tree structure; (2) create new file, add or delete groups and datasets; (3) view and modify the content of a dataset; 4) add, delete and modify attributes; (4) replace I/O and GUI components such as table view, image view and metadata view.
- **read_h5**: The software read_h5 is written in the C language. Users will need the HDF5 libraries when compiling the source code. The program allows users to select a parameter, latitude range, and dump the data to screen as an ASCII file.
- **atmos_h5:** The software atmos_h5 is an IDL-based code. This program not only creates the parameter subsets (with the option of converting data to geophysical parameters) and writes in ASCII or binary format, it also displays the quick-look image on the screen and creates a .jpg file.
- **Giovanni:** A web-based on-line visualization and analysis tool developed for display, data mining and direct download of the selected parameter (for Level 2 or Level 3 products).

For a complete list of tools, please refer to: http://disc.gsfc.nasa.gov/Aura/tools.shtml.

A good overview on tools to read OMI data, including IDL program code and an IDL level 2 analysis toolkit (CAMA) is available from http://www.knmi.nl/omi/research/product/read_tool_omi_level2.html.

5.4 Example of Usage

1. Go to http://disc.gsfc.nasa.gov/Aura/tools.shtml.
2. Click on "OMI-Giovanni." Two types of OMI online visualization and analysis are available: Aura OMI daily global 1.0° x 1.0° and 0.25° x 0.25° products and Aura OMI Level 2G daily global products.
3. Click on the product of interest.
4. Choose any of the parameters: Column Amount Ozone, UV Aerosol Index, or Radiative Cloud Fraction.
5. Optionally, choose the range for latitude and longitude, visualization type and time range.
6. Click on "Generate Visualization."

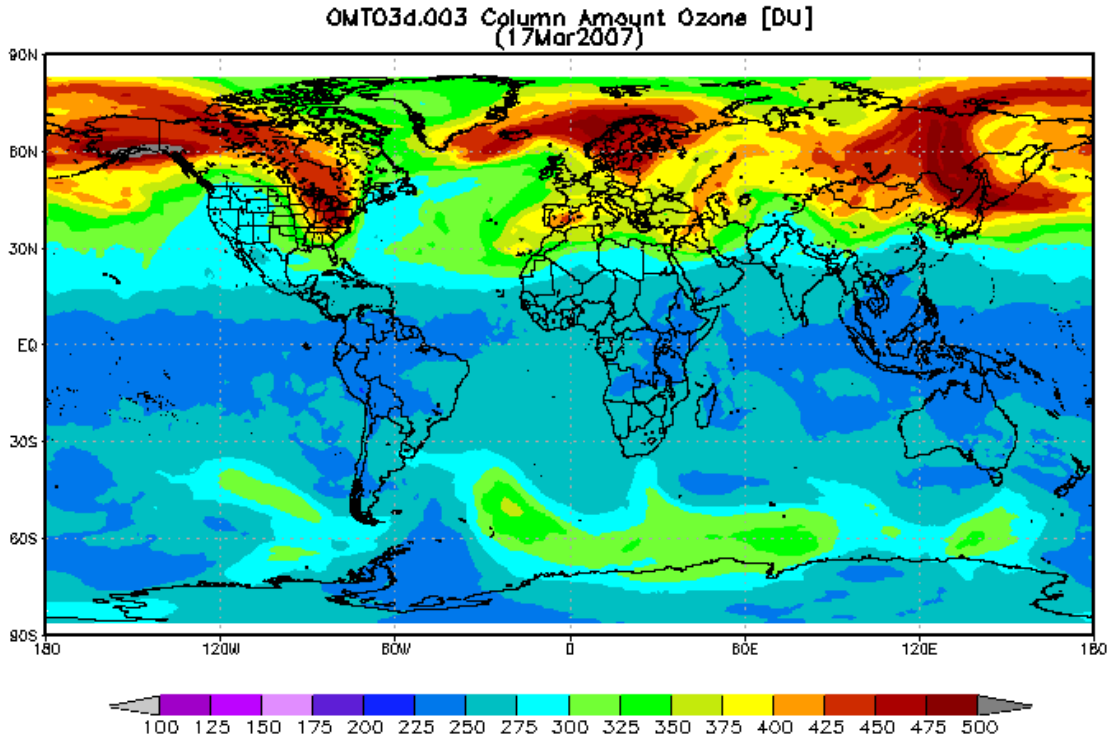

Figure 13: An Image of Column Ozone Generated Using OMI-Giovanni

This page is blank to preserve correct left-right pagination.

Chapter 6: References

6.1 OMI Algorithmic Theoretical Baseline Documents (ATBDs)

OMI ATBD, Volume 1: *OMI Instrument Description and Level 1B Product*
http://eospso.gsfc.nasa.gov/eos_homepage/for_scientists/atbd/docs/OMI/ATBD-OMI-01.pdf

OMI ATBD, Volume 2: *OMI Ozone Products*
http://eospso.gsfc.nasa.gov/eos_homepage/for_scientists/atbd/docs/OMI/ATBD-OMI-02.pdf

OMI ATBD, Volume 3: *Clouds, Aerosols, and Surface UV Irradiance*
http://eospso.gsfc.nasa.gov/eos_homepage/for_scientists/atbd/docs/OMI/ATBD-OMI-03.pdf

OMI ATBD, Volume 4: *OMI Trace Gas Algorithms*
http://eospso.gsfc.nasa.gov/eos_homepage/for_scientists/atbd/docs/OMI/ATBD-OMI-04.pdf

OMI ATBD, Terms and Symbols
http://eospso.gsfc.nasa.gov/eos_homepage/for_scientists/atbd/docs/OMI/ATBD-OMI-Terms-Symbols.pdf

6.2 Additional References

KNMI website: http://www.knmi.nl/omi/research/documents

Acarreta, J.R. and J.F. de Haan, "Cloud Pressure Algorithm Based on O_2-O_2 Absorption," Algorithm Theoretical Baseline Document: *Clouds, Aerosols, & Surface UV Irradiance*, P. Stammes (ed.), Vol. III, ATBD-OMI-03, Version 2.0, Aug. 2002. (http://eospso.gsfc.nasa.gov/eos_homepage/for_scientists/atbd/docs/OMI/ATBD-OMI-03.pdf)

Ahmad, S.P., P. F. Levelt, P. K. Bhartia, E. Hilsenrath, G. W. Leppelmeierd, and J. E. Johnson. Atmospheric products from the ozone monitoring instrument (OMI). In Proc. SPIE, Earth Observing Systems VIII, volume 5151, pages 619–630. William L. Barnes, 2003.

Ahn, C., O. Torres, and P.K. Bhartia, "Comparison of Ozone Monitoring Instrument UV Aerosol Products with Aqua/Moderate Resolution Imaging Spectroradiometer and Multiangle Imaging Spectroradiometer observations in 2006." *J. Geophys. Res.*, 113, D16S27, doi:10.1029/2007JD008832, 2008.

Balis, D., M. Kroon, M. E. Koukouli, E. J. Brinksma, G. Labow, J. P. Veefkind, and R. D. McPeters (2007), Validation of Ozone Monitoring Instrument total ozone column measurements using Brewer and Dobson spectrophotometer ground-based observations, *J. Geophys. Res.*, 112, D24S46, doi:10.1029/2007JD008796.

Bhartia, P.K. and C.W. Wellemeyer, "OMI TOMS-V8 Total O_3 Algorithm," Algorithm Theoretical Baseline Document: *OMI Ozone Products*, P.K. Bhartia (ed.), Vol. II, ATBD-OMI-02, Version 2.0, Aug. 2002. (http://eospso.gsfc.nasa.gov/eos_homepage/for_scientists/atbd/docs/OMI/ATBD-OMI-02.pdf)

Boersma, F., E. Bucsela, E. Brinksma, and J.F. Gleason, "NO_2," Algorithm Theoretical Baseline Document: *OMI Trace Gas Algorithms*, K. Chance (ed.), Vol. IV, ATBD-OMI-04, Version 2.0, Aug. 2002.

Carn, S.A., N.A. Krotkov, K. Yang, R.M. Hoff, A.J. Prata, A.J. Krueger, S.C. Loughlin, and P.F. Levelt (2007b). "Extended observations of volcanic SO_2 and sulfate aerosol in the stratosphere," *Atmos. Chem. Phys. Discuss.*, 7, 2857-2871, 2007. (http://www.atmos-chem-phys-discuss.net/7/2857/2007/acpd-7-2857-2007.pdf)

Carn, S.A., A.J. Krueger, N.A. Krotkov, S. Arellano, and K. Yang. Daily monitoring of Ecuadorian volcanic degassing from space, J. Volcanol. Geotherm. Res., 176(1), 141-150, doi:10.1016/j.jvolgeores.2008.01.029, 2008.

Carn, S.A., A.J. Krueger, N.A. Krotkov, K. Yang, and K. Evans. Tracking volcanic sulfur dioxide clouds for aviation hazard mitigation. Natural Hazards, doi:10.1007/s11069-008-9228-4 (in press), 2009.

Carn, S. A., A.J. Krueger, N. A. Krotkov, K. Yang, and P.F. Levelt, (2007a) "Sulfur dioxide emissions from Peruvian copper smelters detected by the Ozone Monitoring Instrument," *Geophys. Res. Lett.*, 34, L09801, doi:10.1029/2006GL029020, 2007.

Chance, K., T.P. Kurosu, and L.S. Rothman, "HCHO," "OClO," "BrO," Algorithm Theoretical Baseline Document: *OMI Trace Gas Algorithms*, K. Chance (ed.), Vol. IV, ATBD-OMI-04, Version 2.0, Aug. 2002. (http://eospso.gsfc.nasa.gov/eos_homepage/for_scientists/atbd/docs/OMI/ATBD-OMI-04.pdf)

Celarier, E. A., E. J. Brinksma, J. F. Gleason, J. P. Veefkind, A. Cede, J. R. Herman, D. Ionov, F. Goutail, J-P. Pommereau, J.-C. Lambert, M. van Roozendael, G. Pinardi, F. Wittrock, A. Schönhardt, A. Richter, O. W. Ibrahim, T. Wagner, B. Bojkov, G. Mount, E. Spinei, C. M. Chen, T. J. Pongetti, S. P. Sander, E. J. Bucsela, M. O. Wenig, D. P. J. Swart, H. Volten, M. Kroon, and P. F. Levelt, , Validation of Ozone Monitoring Instrument nitrogen dioxide columns, *J. Geophys. Res.*, 113, D15S15,

doi:10.1029/2007JD008908, 2008.

Curier, R.L., J.P. Veefkind, R. Braak, O.Torres, G. de Leeuw, "Retrieval of Aerosols Optical Properties from OMI Rradiances Using a Multi-Wavelength Algorithm: Application and Validation to Western Europe," *Journal of Geophysics Research*, 2007.

Dobber, M.R., R. Dirksen, P. Levelt, G.H.J. van den Oord, R. Voors, Q. Kleipool, G. Jaross, M. Kowalewski, E. Hilsenrath, G. Leppelmeier, J. de Vries, W. Dierssen, and N. Rozemeijer, "Ozone Monitoring Instrument Calibration," *IEEE Trans. Geo. Rem. Sens.*, 2006, Vol. 44, No. 5, 1209-1238.
(http://ieeexplore.ieee.org/search/wrapper.jsp?arnumber=1624601)

Dutch Space, "Output Products and Metadata," *GDPS Input/Output Data Specification* (*IODS*), Vol. 2, SD-OMIE-7200-DS-467, April 9, 2003.

Froidevaux L. and A. Douglass, "Earth Observing System (EOS) Aura Science Data Validation Plan," July 2001.
(http://aura.gsfc.nasa.gov/images/project/aura_validation_v1.0.pdf)

Joiner, J. and A.P. Vasilkov, "First Results from the OMI Rotational Raman Scattering Cloud Pressure Algorithm", *IEEE Trans. Geo. Rem. Sens.*, Vol. 44, No. 5, 1272-1282, 2006. (http://ieeexplore.ieee.org/search/wrapper.jsp?arnumber=1624606)

Joiner, J., A.P. Vasilkov, D. Flittner, E. Buscela, and J. Gleason, "Retrieval of Cloud Pressure from Rotational Raman Scattering," Algorithm Theoretical Baseline Document: *Clouds, Aerosols, and Surface UV Irradiance*, P. Stammes (ed.), Vol. III, ATBD-OMI-03, Ver. 2.0, Aug. 2002.

Joiner, J., A.P. Vasilkov, D.E. Flittner, J.F. Gleason, P.K. Bhartia, "Retrieval of Cloud Pressure and Oceanic Chlorophyll Content Using Raman Scattering in GOME Ultraviolet Spectra," *J. Geophys. Res.*, 2004, Vol. 109, D01109.
(http://www.agu.org/pubs/crossref/2004/2003JD003698.shtml)

Joiner, J., A.P. Vasilkov, K. Yang, G. Labow, P.K. Bhartia, R. Spurr, M. McGill, G. Heymsfield, L. Li, L. Tian, E. Browell, "Evaluation of OMI Cloud Pressure from Rotational Raman Scattering Using Aircraft and Satellite Data," presented at the Aura Science Team Meeting, Boulder, Colorado, USA, September 11-15, 2006.
(http://code916.gsfc.nasa.gov/People/Joiner/Aura_Val_06_v2.ppt)

Kroon, M., I. Petropavlovskikh, R. Shetter, S. Hall, K. Ullmann, J. P. Veefkind, R. D. McPeters, E. V. Browell, and P. F. Levelt (2008), OMI total ozone column validation with Aura-AVE CAFS observations, *J. Geophys. Res.*, 113, D15S13, doi:10.1029/2007JD008795.

Kroon, M., J. P. Veefkind, M. Sneep, R. D. McPeters, P. K. Bhartia, and P. F. Levelt

(2008), Comparing OMI-TOMS and OMI-DOAS total ozone column data, *J. Geophys. Res.*, 113, D16S28, doi:10.1029/2007JD008798.

Krotkov, N.A., P. K. Bhartia, J. R. Herman, V. Fioletov, and J. Kerr, ''Satellite estimation of spectral surface UV irradiance in the presence of tropospheric aerosols 1. Cloud-free case,'' *J. Geophys. Res.,* 103, 8779–8793, 1998.

Krotkov, N.A., J. R. Herman, P. K. Bhartia, V. Fioletov, and Z. Ahmad, ''Satellite estimation of spectral surface UV irradiance 2. Effects of homogeneous clouds and snow,'' *J. Geophys. Res.*, 106, 11743–11759, 2001.

Krotkov, N.A., S.A. Carn, A.J. Krueger, P.K. Bhartia, and K. Yang, "Band Residual Difference Algorithm for Retrieval of SO_2 from the AURA Ozone Monitoring Instrument (OMI)," *IEEE Trans. Geo. Rem. Sens.*, Vol. 44, No. 5, 1259-1266, 2006. (doi:10.1109/TGRS.2005.861932)
or (http://ieeexplore.ieee.org/search/wrapper.jsp?arnumber=1624604)

Krotkov, N.A., J. Herman, P.K. Bhartia, C. Seftor, A. Arola, J. Kaurola, P. Taalas, and A. Vasilkov, "OMI Surface UV Irradiance Algorithm," Algorithm Theoretical Baseline Document: *Clouds, Aerosols, and Surface UV Irradiance*, P. Stammes (ed.), Vol. III, ATBD-OMI-03, Version 2.0, Aug. 2002.

Krotkov, N.A., A. Krueger, K. Yang, S. Carn, P.K. Bhartia, and P. Levelt, "SO_2 Data from the Ozone Monitoring Instrument (OMI)," in *Proceedings of the ENVISAT Symposium*, 2007, 23-27 April 2007, Montreux, Switzerland (July 2007), H. Lacoste & L. Ouwehand (Eds.), ESA SP-636 //CD (2 volumes).

Krotkov, N.A., B. McClure, R. Dickerson, S. Carn, Can Li, P.K. Bhartia, K. Yang, A. Krueger, Z. Li, J. Hains, P. Levelt, H. Chen, J. Yuan, F. Gong, and X. Bian, "Validation of SO2 retrievals from the Ozone Monitoring Instrument over NE China," *J. Geophys. Res.*, 113, D16S40, doi:10.1029/2007JD008818, 2008.

Krueger, A.J., N.A. Krotkov, S. Datta, D. Flittner, and O. Dubovik, "SO_2," Algorithm Theoretical Baseline Document: *OMI Trace Gas Algorithms*, K. Chance (ed.), Vol. IV, ATBD-OMI-04, Version 2.0, Aug. 2002.

Krueger, A.J., L.S. Walter, P.K. Bhartia, C.C. Schnetzler, N.A. Krotkov, I. Sprod, and G.J.S. Bluth. (1995) Volcanic sulfur dioxide measurements from the Total Ozone Mapping Spectrometer (TOMS) Instruments. Journal of Geophysical Research, 100, D7, 14,057 - 14,076.

Kurosu, T.P., K. Chance, and C.E. Sioris, "Preliminary Results for HCHO and BrO from the EOS-Aura Ozone Monitoring Instrument," *Passive Optical Remove Sensing of the Atmosphere and Clouds IV*, S.C. Tsay, T. Yokota, and M.-H. Ahn (Eds.), *Proc. of SPIE*, 2004, Vol. 5652 (SPIE, Bellingham, WA, 2004), 0277-786X/04/$15.
(http://cfa-www.harvard.edu/~tkurosu/Papers/SPIE_2004.pdf)

Levelt, P.F., E. Hilsenrath, G.W. Leppelmeier, G.H.J. van den Oord, P.K. Bhartia, J. Tamminen, J.F. de Haan and J.P. Veefkind, "Science Objectives of the Ozone Monitoring Instrument," *IEEE Trans. Geo. Rem. Sens.*, Vol. 44, No. 5, 1199-1208, 2006. (http://ieeexplore.ieee.org/search/wrapper.jsp?arnumber=1624600).

McPeters, R., M. Kroon, G. Labow, E. Brinksma, D. Balis, I. Petropavlovskikh, J. P. Veefkind, P. K. Bhartia, and P. F. Levelt (2008), Validation of the Aura Ozone Monitoring Instrument total column ozone product, *J. Geophys. Res.*, 113, D15S14, doi:10.1029/2007JD008802.

Tanskanen, A., A. Lindfors, A. Maatta, N. Krotkov, J. Herman, J. Kaurola, T. Koskela, K. Lakkala, V. Fioletov, J. Bernhard, R. McHenzie, Y. Kondo, M. O'Neill, H. Slaper, P. den Outer, A.F. Bais, and J. Tamminen, "Validation of daily erythemal doses from OMI with ground-based UV measurement data", *J. Geophys. Res.*, 112, D24S44, doi:10.1029/2007JD008830, 2007.

Torres, O., R. Decae, J.P. Veefkind, and G. de Leeuw, "OMI Aerosol Retrieval Algorithm," Algorithm Theoretical Baseline Document: *Clouds, Aerosols, and Surface UV Irradiance*, P. Stammes (ed.), Vol. III, ATBD-OMI-03, Version 2.0, Aug. 2002.

Torres, O., A. Tanskanen, B. Veihelmann, C. Ahn, R. Braak, P.K. Bhartia, P. Veefkind, and P. Levelt, "Aerosols and surface UV products from Ozone Monitoring Instrument observations: An overview," *J. Geophys. Res.*, 112, D24S47, 2007. (doi:10.1029/2007JD008809)

Torres, O., C. Ahn, M. Andrade, and T. Eck, "Evaluation of OMI UV Aerosol Products Using AERONET Observations," *J. Geophys. Res.*, submitted manuscript, 2008.

Shavrina, A. V., Y. V. Pavlenko, A. Veles, I. Syniavskyi, and M. Kroon (2007), Ozone columns obtained by ground-based remote sensing in Kiev for Aura Ozone Measuring Instrument validation, *J. Geophys. Res.*, 112, D24S45, doi:10.1029/2007JD008787.

Sneep, M., J.F. de Haan, P. Stammes, P. Wang, C. Vanbauce, J. Joiner, A.P. Vasilkov and P.F. Levelt, Three way comparison between OMI and PARASOL cloud pressure products, J. Geophys. Res., 2008, 113, doi:10.1029/2007JD008694.

Stammes, P., M. Sneep, J.F. de Haan, J.P. Veefkind, P. Wang and P.F. Levelt, Effective cloud fractions from the Ozone Monitoring Instrument: Theoretical framework and validation, J. Geophys. Res., 2008, 113, doi:10.1029/2007JD008820.

van den Oord, G.H.J., R.H.M. Voors, and J. de Vries, "The Level 0 to Level 1B Processor for OMI Radiance, Irradiance and Calibration Data," Algorithm Theoretical Baseline Document: *OMI Instrument, Level 0-1B Processor, Calibration & Operations*, P.F. Levelt (ed.), Vol. I, ATBD-OMI-01, Version 2, Aug. 2002.

van den Oord, G.H.J., J. P. Veefkind, P. F. Levelt, M. R. Dobber, "Level 0 to 1B Processing and Operational Aspects," IEEE Trans. Geosc. Rem. Sens. 44 (5), pp 1380-1397, 2006.

van Oss, R.F., R.H.M. Voors, and R.D.J. Spurr, "Ozone Profile Algorithm," Algorithm Theoretical Baseline Document: *OMI Ozone Products*, P.K. Bhartia (ed.), Vol. II, ATBD-OMI-02, Version 2.0, Aug. 2002.

Vasilkov, A.P., J. Joiner, K. Yang, and P.K. Bhartia, "Improving Total Column Ozone Retrievals by Using Cloud Pressures Derived from Raman Scattering in the UV," *Geophys. Res. Lett.*, 2004, Vol. 31, L20109.
(http://www.agu.org/pubs/crossref/2004/2004GL020603.shtml)

Vasilkov, A., J. Joiner, R. J. D. Spurr, P. K. Bhartia, P. Levelt, and G. L. Stephens (2008), "Evaluation of the OMI cloud pressures derived from rotational Raman scattering by comparisons with other satellite data and radiative transfer simulations, *J. Geophys. Res.*, 113, D15S19, doi:10.1029/2007JD008689,"

Veefkind, J.P., and J.F. de Haan, "DOAS Total O_3 Algorithm," Algorithm Theoretical Baseline Document: *OMI Ozone Products*, P.K. Bhartia (ed.), Vol. II, ATBD-OMI-02, Version 2.0, Aug. 2002.

Veefkind, J.P., J.F. de Haan, E.J. Brinksma, M. Kroon and P.F. Levelt, "Total Ozone from the Ozone Monitoring Instrument (OMI) Using the DOAS Technique," *IEEE Trans. Geo. Rem. Sens.*, Vol. 44, No. 5, 1239-1244, 2006.
(http://ieeexplore.ieee.org/search/wrapper.jsp?arnumber=1624602)

Veihelmann, B., P.F. Levelt., P. Stammes, and J.P. Veefkind: Simulation study of the aerosol information content in OMI spectral reflectance measurements, Atmos. Chem. Phys., 7, 3115-3127, 2007.

Yang, K., N. A. Krotkov, A. J. Krueger, S. A. Carn, P. K. Bhartia, and P. F. Levelt, "Retrieval of large volcanic SO2 columns from the Aura Ozone Monitoring Instrument: Comparison and Limitations," *J. Geophys. Res.*, 112, D24S43, doi:10.1029/2007JD008825, 2007.

Yang, K., N.A. Krotkov, A.J. Krueger, S.A. Carn, P.K. Bhartia, and P.F Levelt, "Improving retrieval of volcanic sulfur dioxide from backscattered UV satellite observations", *Geophys. Res. Lett.*, 36, L03102, doi:10.1029/2008GL036036, 2009.